

1 Estimating winter balance and its uncertainty from direct 2 measurements of snow depth and density on alpine glaciers

3 Alexandra PULWICKI,¹ Gwenn E. FLOWERS,¹ Valentina RADIC²,² [Derek](#)
4 [BINGHAM](#)³

5 ¹ *Department of Earth Sciences, Simon Fraser University, Burnaby, BC, Canada*

6 ²*Department of Earth, Ocean and Atmospheric Sciences, University of British Columbia, Vancouver, BC,*
7 *Canada*

8 ³ *Department of Statistics and Actuarial Science, Simon Fraser University, Burnaby, BC, Canada*

9 *Correspondence: Alexandra Pulwinski <apulwick@sfu.ca>*

10 **ABSTRACT.** Accurately estimating winter surface mass balance on glaciers
11 is central to assessing glacier health and predicting glacier runoff. However,
12 measuring and modelling snow distribution is inherently difficult in moun-
13 tainous terrain. Here we explore rigorous statistical methods of estimating
14 winter balance and its uncertainty from multiscale measurements of snow
15 depth and density. In May 2016 we collected over 9000 manual measurements
16 of snow depth across three glaciers in the St. Elias Mountains, Yukon,
17 Canada. Linear regression, combined with cross correlation and Bayesian
18 model averaging, as well as ordinary kriging are used to interpolate point-
19 scale values to glacier-wide estimates of winter balance. Elevation and a wind-
20 redistribution parameter exhibit the highest correlations with winter balance,
21 but the relationship varies considerably between glaciers. A Monte Carlo
22 analysis reveals that the interpolation itself introduces more uncertainty than
23 the assignment of snow density or the representation of grid-scale variability.
24 For our study glaciers, the winter balance uncertainty from all assessed sources
25 ranges from 0.03 m w.e. (8%) to 0.15 m w.e. (54%). Despite the challenges

associated with estimating winter balance, our results are consistent with a regional-scale winter-balance gradient.

INTRODUCTION

Winter surface mass balance, or “winter balance”, is the net accumulation and ablation of snow over the winter season (Cogley and others, 2011), which constitutes glacier mass input. Winter balance (B_w) is half of the seasonally resolved mass balance, initializes summer ablation conditions and must be estimated to simulate energy and mass exchange between the land and atmosphere (e.g. Hock, 2005; Réveillet and others, 2016). Effectively representing the spatial distribution of snow on glaciers is also central to monitoring surface runoff and its downstream effects (e.g. Clark and others, 2011).

Winter balance (WB) is notoriously difficult to estimate (e.g. Dadić and others, 2010; Cogley and others, 2011). Snow distribution in alpine regions is highly variable with short correlation length scales (e.g. Anderton and others, 2004; Egli and others, 2011; Grünwald and others, 2010; Helbig and van Herwijnen, 2017; López-Moreno and others, 2011, 2013; Machguth and others, 2006; Marshall and others, 2006) and is influenced by dynamic interactions between the atmosphere and complex topography, operating on multiple spatial and temporal scales (e.g. Barry, 1992; Liston and Elder, 2006; Clark and others, 2011) (e.g. Barry, 1992; Liston and Elder, 2006; Clark and others, 2011; Scipión and others, 2013). Simultaneously extensive, high resolution and accurate snow distribution measurements on glaciers are therefore difficult to obtain (e.g. Cogley and others, 2011; McGrath and others, 2015). Physically based models are acquire (e.g. Cogley and others, 2011; McGrath and others, 2015) and obtaining such measurements is further complicated by the inaccessibility of many glacierized regions during the winter. Use of physically based models to estimate winter balance is computationally intensive and require requires detailed meteorological data to drive them the models (Dadić and others, 2010). As a result, there is significant uncertainty in estimates of winter balance, thus limiting the ability of models to represent current and projected glacier conditions.

Studies that have focused on obtaining detailed estimates of WB B_w have used a wide range of observational techniques, including direct measurement of snow depth and density (e.g. Cullen and others, 2017), lidar or photogrammetry (e.g. Sold and others, 2013) and ground-penetrating radar (e.g. Machguth and others, 2006; Gusmeroli and others, 2014; McGrath and others, 2015). Spatial coverage of direct measurements is generally limited and often comprises an elevation transect along the glacier centreline

(e.g. Kaser and others, 2003). Measurements are ~~often~~typically interpolated using linear regression on only a few topographic parameters (e.g. MacDougall and Flowers, 2011), with elevation being the most common. Other established techniques include hand contouring (e.g. Tangborn and others, 1975), kriging (e.g. Hock and Jensen, 1999) and attributing measured winter balance values to elevation bands (e.g. Thibert and others, 2008). Physical snow models have been used to estimate spatial patterns of winter balance (e.g. Mott and others, 2008; Schuler and others, 2008; Dadić and others, 2010), but availability of the required meteorological data generally prohibits their widespread application. Error analysis is rarely undertaken and few studies have thoroughly investigated uncertainty in spatially distributed estimates of winter balance (c.f. Schuler and others, 2008).

More sophisticated snow-survey designs and statistical models of snow distribution are widely used in the field of snow science. Surveys described in the snow science literature are generally spatially extensive and designed to measure snow depth and density throughout a basin, ensuring that all terrain types are sampled. A wide array of measurement interpolation methods are used, including linear (e.g. López-Moreno and others, 2010) and non-linear regressions (e.g. Molotch and others, 2005) that include numerous terrain parameters, as well as geospatial interpolation ~~(e.g. Erxleben and others, 2002)~~ (e.g. Erxleben and others, 2002; Cullen and others, 2017) including various forms of kriging. Different interpolation methods are also combined; for example, regression kriging (see Supplementary Material) adds kriged residuals to a field obtained with linear regression (e.g. Balk and Elder, 2000). Physical snow models such as SnowTran-3D (Liston and Sturm, 1998), Alpine3D (Lehning and others, 2006) and SnowDrift3D (Schneiderbauer and Prokop, 2011) are widely used, and errors in estimating snow distribution have been examined from theoretical (e.g. Trujillo and Lehning, 2015) and applied perspectives (e.g. Turcan and Loijens, 1975; Woo and Marsh, 1978; Deems and Painter, 2006).

The goals of this study are to (1) critically examine methods of converting direct snow depth and density measurements to distributed estimates of winter balance; and (2) identify sources of uncertainty, evaluate their magnitude and assess their combined contribution to uncertainty in glacier-wide winter balance. We focus on commonly applied, low-complexity methods of measuring and estimating winter balance in the interest of making our results broadly applicable.

STUDY SITE

The St. Elias Mountains (Fig. 1a) rise sharply from the Pacific Ocean, creating a significant climatic gradient between coastal maritime conditions, generated by Aleutian–Gulf of Alaska low-pressure

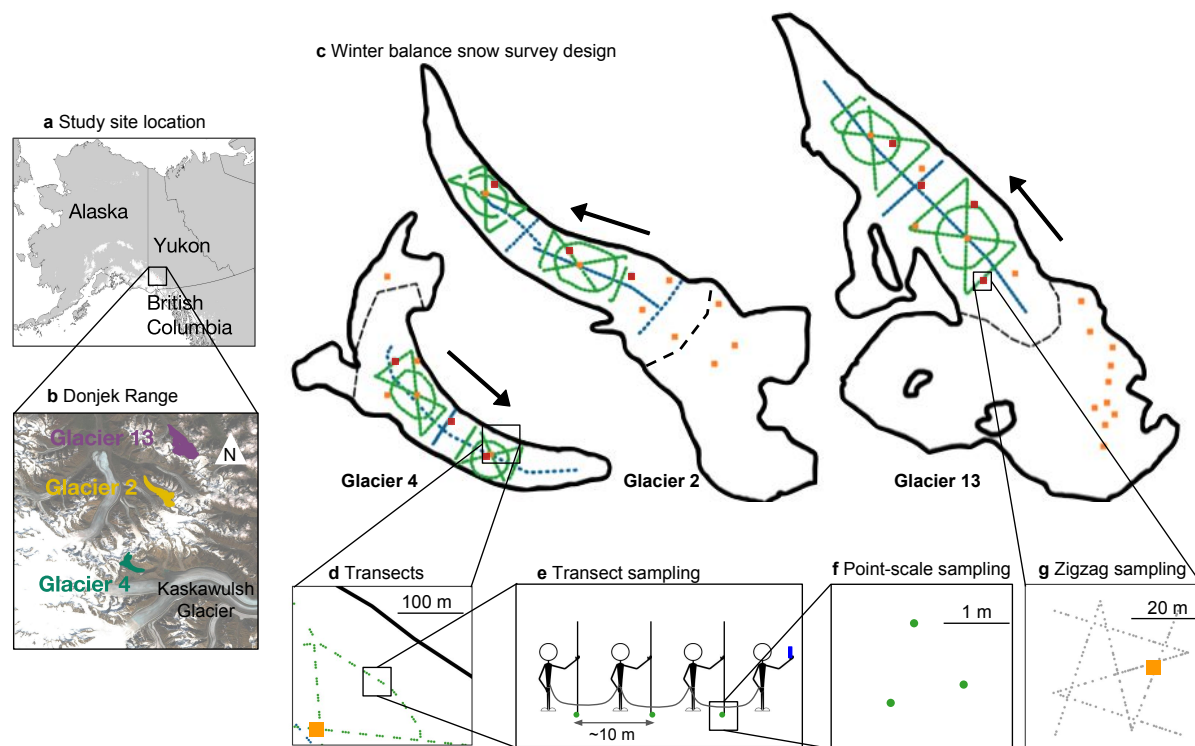


Fig. 1. Study area location and sampling design for Glaciers 4, 2 and 13. (a) Study region in the Donjek Range of the St. Elias Mountains of Yukon, Canada. (b) Study glaciers located along a southwest-northeast-southwest-northeast transect through the Donjek Range. The local topographic divide is shown as a dashed line. Imagery from Landsat8 (5 September 2013, data available from the U.S. Geological Survey). (c) Details of the snow-survey sampling design, with centreline and transverse transects (blue dots), hourglass and circle designs (green dots) and locations of snow density measurements (orange squares). Arrows indicate ice-flow directions. Approximate location of ELA on each glacier is shown as a black dashed line. (d) Close up of linear and curvilinear transects. (e) Configuration of navigator and observers. (f) Point-scale snow-depth sampling. (g) Linear-random snow-depth measurements in ‘zigzag’ design (grey-red dots) with one density measurement (orange square) per zigzag.

85 systems, and interior continental conditions, driven by the Yukon–Mackenzie high-pressure system
 86 (Taylor-Barge, 1969). The boundary between the two climatic zones is generally aligned with the divide
 87 between the Hubbard and Kaskawulsh Glaciers, approximately 130 km from the coast. Research on snow
 88 distribution and glacier mass balance in this area is limited. A series of research programs, including
 89 Project “Snow Cornice” and the Icefield Ranges Research Project, were operational in the 1950s and
 90 60s (Wood, 1948; Danby and others, 2003) and in the last 30 years, there have been a few long-term
 91 studies on selected alpine glaciers (e.g. Clarke, 2014) as well as several regional studies of glacier mass
 92 balance and dynamics (e.g. Arendt and others, 2008; Burgess and others, 2013; Waechter and others, 2015)

Table 1. Physical characteristics of the study glaciers and May 2016 winter balance survey details, including number of snow depth measurement locations along transects (n_T), total length of transects (d_T), number of combined snow pit and Federal Sampler density measurement locations (n_P) and number of zigzag surveys (n_{zz}).

	Location	Location	Elevation (m a.s.l)			Slope (°)	Area	
	UTM Zone 7	UTM Zone 7	Mean	Range	ELA	Mean	$n_T d_T$ (km ²)	$n_P n_{zz}$
height	595470 E	6740730 N	2344	1958–2809	~2500	12.8	3.8	4
Glacier 4							7 May 2016	649
Glacier 2	601160 E	6753785 N	2495	1899–3103	~2500	13.0	7.0	8
Glacier 13	604602 E	6763400 N	2428	1923–3067	~2380	13.4		11
								3
							12.6	

(e.g. Arendt and others, 2008; Berthier and others, 2010; Burgess and others, 2013; Waechter and others, 2015)

We carried out winter balance surveys on three unnamed glaciers in the Donjek Range of the St. Elias Mountains. The Donjek Range is located approximately 40 km to the east of the regional mountain divide and has an area of about 30×30 km². Glacier 4, Glacier 2 and Glacier 13 (labelling adopted from Crompton and Flowers (2016)) are located along a southwest-northeast transect through the range (Fig. 1b, Table 1). These small alpine glaciers are generally oriented southeast-northwest, with Glacier 4 having a predominantly southeast aspect and Glaciers 2 and 13 have generally northwest aspects. The glaciers are situated in valleys with steep walls and have simple geometries. Based on a detailed study of Glacier 2 (Wilson and others, 2013) and related theoretical modelling (Wilson and Flowers, 2013) we suspect all of the study glaciers to be polythermal.

METHODS

Estimating glacier-wide winter balance (B_w) involves transforming measurements of snow depth and density into values of winter balance distributed across a defined grid (b_w). We do this in four steps. (1) Obtain direct measurements of snow depth and density in the field. (2) Assign density values to all depth-measurement locations to calculate point-scale values of WB at each location. (3) Average all point-scale values of b_w within each gridcell of a digital elevation model (DEM) to obtain the gridcell-averaged WB . (4) Interpolate and extrapolate these gridcell-averaged WB values to obtain estimates of WB (in m w.e.) in b_w in each gridcell across the domain. B_w is then calculated by taking the average of all gridcell-averaged b_w values for each glacier. For brevity, we refer to these four

Table 2. Details of the May 2016 winter-balance survey, including number of snow-depth measurement locations along transects (n_T), total length of transects (d_T), number of combined snow pit and Federal Sampler density measurement locations (n_ρ), number of zigzag surveys (n_{zz}), number (as percent of total number of gridcells, and of the number of gridcells in the ablation area) of gridcells sampled (n_S) and the elevation range (as percent of total elevations range and of ablation-area elevation range).

	Date	n_T	d_T (km)	n_ρ	n_{zz}	n_S	Elevation range (m a.s.l.)
Glacier 4	4–7 May 2016	649	13.1	7	3	295 (12%, 21%)	2015–2539 (62%, 97%)
Glacier 2	8–11 May 2016	762	13.6	7	3	353 (8%, 14%)	2151–2541 (32%, 47%)
Glacier 13	12–15 May 2016	941	18.1	20 19	4	468 (6%, 14%)	2054–2574 (45%, 62%)

steps as (1) field measurements, (2) density assignment, (3) gridcell-averaged $\text{WB-}b_w$ and (4) distributed $\text{WB-}b_w$. Detailed methodology for each step is outlined below. We use the SPIRIT SPOT-5 DEM (40×40 m) from 2005 (Korona and others, 2009) throughout this study.

Field measurements

Our sampling campaign involved four people and occurred between 5–15 May 2016, which falls within the period of historical peak snow accumulation in southwestern Yukon (Yukon Snow Survey Bulletin and Water Supply Forecast, May 1, 2016). Snow depth is generally accepted to be more variable than density (Elder and others, 1991; Clark and others, 2011; López-Moreno and others, 2013) so we chose a sampling design that resulted in a high ratio (~55:1) of snow depth to density measurements. In total, we collected more than 9000 snow-depth measurements and more than 100 density measurements throughout the study area (Table 1).

During the field campaign there were two small accumulation events. The first, on 6 May 2016, also involved high winds so accumulation could not be determined. The second, on 10 May 2016, resulted in 0.01 m w.e accumulation measured at one location on Glacier 2. Assuming both accumulation events contributed a uniform 0.01 m w.e accumulation to all study glaciers then our survey did not capture ~3% and ~2% of estimated B_w on Glaciers 4 and 2, respectively. We therefore assume that these accumulation events were negligible and apply no correction. Positive temperatures and clear skies occurred between 11–16 May 2016, which we suspect resulted in melt occurring on Glacier 13. The snow in the lower part of the ablation area

of Glacier 13 was isothermal and showed clear signs of melt and metamorphosis. The total amount of melt during the study period was estimated using a degree-day model and found to be small (≤ 0.01 m w.e., see Supplementary Material) so no corrections were made.

Sampling design

The snow surveys were designed to capture variability in snow depth at regional, basin, gridcell and point scales (Clark and others, 2011). To capture variability at the regional scale we chose three glaciers along a transect aligned with the dominant precipitation gradient (Fig. 1b) (Taylor-Barge, 1969). To account for basin-scale variability, snow depth was measured along linear and curvilinear transects on each glacier (Fig. 1c) with a sample spacing of 10–60 m (Fig. 1d). Sample spacing was constrained by protocols for safe glacier travel, while survey scope was constrained by the need to complete all surveys within the period of peak accumulation. We selected centreline and transverse transects as the most commonly used survey designs in winter balance studies (e.g. Kaser and others, 2003; Machguth and others, 2006) as well as an hourglass pattern with an inscribed circle, which allows for sampling in multiple directions and easy travel (personal communication from C. Parr, 2016). To capture variability at the grid scale, we densely sampled up to four gridcells on each glacier using a linear-random sampling design (Shea and Jamieson, 2010) we term a ‘zigzag’. To capture point-scale variability, each observer made 3–4 depth measurements within ~ 1 m (Fig. 1ef) at each transect measurement location. ~~In total, we collected more than 9000 snow-depth measurements throughout the study area (Table 1).~~

Snow depth: transects

~~Winter balance can be estimated as the product of snow depth and depth-averaged density. Snow depth is generally accepted to be more variable than density (Elder and others, 1991; Clark and others, 2011; López-Moreno and others, 2013) so we chose a sampling design that resulted in a high ratio ($\sim 55:1$) of snow depth to density measurements. Our sampling campaign involved four people and occurred between 5–15 May 2016, which falls within the period of historical peak snow accumulation in southwestern Yukon (Yukon Snow Survey Bulletin and Water Supply Forecast, May 1, 2016).~~ While roped-up for glacier travel with fixed distances between observers, the lead observer used a single-frequency GPS unit (Garmin GPSMAP 64s) to navigate between predefined transect measurement locations (Fig. 1e). The remaining three observers used 3.2 m graduated aluminum avalanche probes to make snow-depth measurements (Kinar and Pomeroy, 2015). The locations of each set of depth measurements, made by the second, third and fourth observers, are estimated using the recorded location of the first

observer, the approximate distance between observers and the direction of travel. The 3–4 point-scale depth measurements are averaged to obtain a single depth measurement at each transect measurement location. When considering snow variability at the point scale as a source of uncertainty in snow depth measurements, we find that the mean standard deviation of point-scale snow depth measurements is $<7\%$ of the mean snow depth for all study glaciers.

Snow-depth sampling was concentrated in the ablation area to ensure that only snow from the current accumulation season was measured. The boundary between snow and firn in the accumulation area can be difficult to detect and often misinterpreted, especially when using an avalanche probe (Grünwald and others, 2010; Sold and others, 2013). We intended to use a firn corer to measure winter balance in the accumulation area, but cold snow combined with positive air temperatures led to cores being unrecoverable. Successful snow depth ~~and density~~ measurements within the accumulation area were made either in snow pits or using a Federal Sampler (described below) to unambiguously identify the snow–firn transition.

Snow depth: zigzags

~~To capture snow depth variability within a single DEM gridcell, we implemented a linear-random zigzag sampling design (Shea and Jamieson, 2010).~~ We measured depth at random intervals of 0.3–3.0 m along two ‘Z’-shaped patterns (Shea and Jamieson, 2010), resulting in 135–191 measurements per zigzag, within three to four ~~40 × 40~~ 40 × 40 m gridcells (Fig. 1g) per glacier. Random intervals were machine-generated from a uniform distribution in sufficient numbers that each survey was unique. Zigzag locations were randomly chosen within the upper, middle and lower regions of the ablation area of each glacier. ~~A fourth zigzag was measured~~ Extra time in the field allowed us to measure a fourth zigzag on Glacier 13 in the central ablation area at ~2200 m a.s.l.

Snow density

Snow density was measured using a Snowmetrics wedge cutter in three snow pits on each glacier, ~~as well as with a Geo-Scientific Ltd. metric Federal Sampler.~~ Within the snow pits (SP), we measured a vertical density profile (in ~~5–10~~ cm increments) with the ~~5 × 10 × 10~~ 5 × 5 × 10 cm wedge-shaped cutter (250 cm³) and a Presola 1000 g spring scale ~~(e.g. Gray and Male, 1981; Fierz and others, 2009)~~ (e.g. Gray and Male, 1981; Fierz and others, 2009; Kinar and Pomeroy, 2015). Wedge-cutter error is approximately $\pm 6\%$ (e.g. Proksch and others, 2016; Carroll, 1977). Uncertainty in estimating density from ~~snow-pit~~ SP measurements also stems from incorrect assignment of density to layers that cannot be sampled (e.g. ice lenses and hard layers). We attempt to quantify this uncertainty by varying estimated ice-layer

thickness by ± 1 cm ($\leq 100\%$) of the recorded thickness, ice layer density between 700 and 900 kg m⁻³ and the density of layers identified as being too hard to sample (but not ice) between 600 and 700 kg m⁻³. When considering all three sources of uncertainty, the range of integrated density values is always less than 15% of the reference density. Depth-averaged densities for shallow pits (<50 cm) that contain ice lenses are particularly sensitive to changes in prescribed density and ice-lens thickness.

While ~~snow-pits~~ SP provide the most accurate measure of snow density, digging and sampling a ~~snow pit~~ SP is time and labour intensive. Therefore, a ~~Federal Snow-Geo Scientific Ltd. metric Federal~~ Sampler (FS) (Clyde, 1932) with a 3.2–3.8 cm diameter sampling tube, which directly measures depth-integrated snow-water equivalent, was used to augment the ~~snow-pit~~ SP measurements. A minimum of three ~~Federal Sampler~~ FS measurements were taken at each of 7–19 locations on each glacier and an additional eight ~~Federal Sampler~~ FS measurements were co-located with ~~each snow-pit profile~~ two SP profiles for each glacier. Measurements for which the snow core length inside the sampling tube was less than 90% of the snow depth were discarded. Densities at each measurement location (eight at each ~~snow-pit~~ SP, three elsewhere) were then averaged, with the standard deviation taken to represent the uncertainty.

~~During the field campaign there were two small accumulation events. The first, on 6 May 2016, also involved high winds so accumulation could not be determined. The second, on 10 May 2016, resulted in 0.01 m w.e accumulation measured at one location on Glacier 2. Positive temperatures and clear skies occurred between 11–16 May 2016, which we suspect resulted in melt occurring on Glacier 13. The snow in the lower part of the ablation area of Glacier 13 was isothermal and showed clear signs of melt and metamorphosis. The total amount of accumulation and melt during the study period could not be estimated so no corrections were made.~~ The mean standard deviation of FS-derived density was $\leq 4\%$ of the mean density for all glaciers.

213 Density assignment

Measured snow density must be interpolated or extrapolated to estimate point-scale ~~winter-balance~~ b_w at each snow-depth sampling location. We employ four commonly used methods to interpolate and extrapolate density (Table 3): (1) calculate mean density over an entire mountain range (e.g. Cullen and others, 2017), (2) calculate mean density for each glacier (e.g. Elder and others, 1991; McGrath and others, 2015), (3) linear regression of density on elevation for each glacier (e.g. Elder and others, 1998; Molotch and others, 2005) and (4) calculate mean density using inverse-distance weighting (e.g. Molotch and others, 2005) for each glacier. Densities derived from ~~snow-pit (SP) measurements and the Federal Sampler (FS)~~ SP and

Table 3. Eight methods used to estimate snow density at unmeasured locations. Total number of resulting density values given in parentheses, with n_T the total number of snow-depth measurement locations along transects (Table 1).

Method code	Source of measured snow density		Density assignment method
	<i>Snow pit</i>	<i>Federal</i>	
		<i>Sampler</i>	
S1	■		Mean of measurements
F1		■	across all glaciers (1)
S2	■		Mean of measurements
F2		■	for each glacier (3)
S3	■		Regression of density on
F3		■	elevation for each glacier (n_T)
S4	■		Inverse distance weighted
F4		■	mean for each glacier (n_T)

[FS measurements](#) are treated separately, for reasons explained below, resulting in eight possible methods of assigning density.

Gridcell-averaged winter balance

We average one to six (mean of 2.1 measurements) point-scale values of ~~WB within each 40 × 40 m~~ [b_w within each](#) DEM gridcell to obtain the gricell-averaged ~~WB~~ [b_w](#). The locations of individual measurements have uncertainty due to the error in the horizontal position given by the GPS unit and the estimation of observer location based on the recorded GPS positions of the navigator. This location uncertainty could result in the incorrect assignment of a point-scale ~~WB~~ [b_w measurement](#) to a particular gridcell. However, this source of error is not further investigated because we assume that the uncertainty ~~in gridecell-averaged WB resulting from incorrect locations of point-scale b_w values~~ is captured in the ~~zigzag measurements uncertainty derived from zigzag measurements, as~~ described below. ~~Uncertainty Error~~ due to having multiple observers ~~was also evaluated. There are~~ [is also evaluated by conducting an analysis of variance \(ANOVA\) of snow-depth measurements along a transect \(amounting to 23 hypothesis tests, one for each transect\) and testing for differences between observers. We find](#) no significant differences between snow-depth measurements made by observers along any transect ($p > 0.05$), with the exception of the first transect on Glacier 4 (51 measurements) ~~, where snow depth measurements collected by one observer were, on average, greater than the snow depth~~

measurements taken by the other two observers ($p < 0.01$). Since this was the first transect and the only one to show differences by observer, this difference can be considered an anomaly. We conclude that observer bias is not an important effect in this study and therefore apply no observer corrections to the data.

Distributed winter balance

Gridcell-averaged values of $WB - b_w$ are interpolated and extrapolated across each glacier using linear regression (LR) and simple kriging (SK) ordinary kriging (OK). The regression-LR relates gridcell-averaged WB and b_w to various topographic parameters, as this method. We use this method because it is simple and has precedent for success (e.g. McGrath and others, 2015). Instead of a basic regression standard LR however, we use cross-validation and implemented in such a way as to prevent data overfitting, and employ model averaging to test allow for all combinations of the chosen topographic parameters. We compare the regression approach with simple kriging (SK), a data-driven LR approach with conventional OK, an interpolation method free of any physical interpretation (e.g. Hock and Jensen, 1999) physical interpretation beyond the premise of spatial correlation in the data (e.g. Hock and Jensen, 1999; Rasmussen and Williams, 2006).

Linear regression

In the regression A multiple linear regression takes the form $\mathbf{y} = \mathbf{X}\beta + \epsilon$, where \mathbf{y} is the dependent variable, the matrix \mathbf{X} in our case contains the set of independent regressors (columns) for each spatial location (rows), β is the vector of regression coefficients and ϵ is independent normal white noise with standard deviation σ (e.g. Davis and Sampson, 1986). In the LR, we use commonly applied defined topographic parameters as the regressors as in McGrath and others (2015), including elevation, slope, aspect, curvature, “northness” and a wind-redistribution parameter (Sx from Winstral and others (2002)); we add distance-from-centreline as an additional parameter. Topographic parameters are standardized for use in the LR. The goal of the LR is to obtain a set of fitted regression coefficients β that correspond to each topographic parameter (regressor) and to a model intercept. For details on data and methods used to estimate the topographic parameters see the Supplementary Material and Pulwinski (2017). Our sampling design ensured that the ranges of topographic parameters associated with our measurement locations represent more than 70% of the total area of each glacier (except elevation on Glacier 2, where our measurements captured only 50%). Topographic parameters are standardized and then weighted by a set of fitted regression coefficients (β_i) calculated by minimizing the sum of squares of the vertical deviations of each datum from the regression line (Davis and Sampson, 1986). For details on data and methods used to estimate the topographic parameters see the Supplementary Material.

~~To~~ We use a combination of cross validation and model averaging to avoid overfitting the data ~~and to~~
 incorporate every possible combination of topographic parameters, cross-validation and model averaging are
 implemented. First, cross-validation is used to obtain a set of β_i values that have the greatest predictive ability
~~.-We~~, to account for uncertainty in the selected predictors and to maximize the model's predictive ability
 (Madigan and Raftery, 1994; Kohavi and others, 1995). Since there are 7 predictors, there are 2^7 possible
 subsets of predictors, or equivalently, models. For a given model, we randomly select 1000 subsets of the
 data (where each subset includes $\sim 2/3$ of the values) ~~to fit the LR and data~~ and fit a multiple linear
 regression using least squares (implemented in MATLAB), thus obtaining 1000 sets of β . Distributed b_w is
 then calculated by multiplying the topographic parameters by their corresponding regression coefficients for
 all DEM gridcells. We use the remaining data ($\sim 1/3$ of the values) to calculate a root mean squared error
 (RMSE) ~~(Kohavi and others, 1995)~~ between the estimated and observed b_w at the measurement locations.
 From the 1000 sets of β_i values, we select the set that results in the lowest RMSE. ~~Second, we use model~~
~~averaging to account for uncertainty when selecting predictors and to maximize the model's predictive ability~~
~~(Madigan and Raftery, 1994). Models are generated by calculating a set of β_i as described above for all~~
~~possible combinations of topographic parameters (This set of β has the greatest predictive ability for a~~
~~particular linear combination of topographic parameters. The procedure above is repeated for each of the~~
~~models, giving the best β for each of the 2^7 models).~~ Using a Bayesian framework, model averaging involves
~~weighting all models by their posterior model probabilities (Raftery and others, 1997). To obtain the final~~
~~regression coefficients, the β_i values from each model are weighted according to the~~
 With the β 's in hand, we move on to prediction. To do so, we use Bayesian model averaging. We weight the
 models according to their relative predictive success ~~of the model~~, as assessed by the value of the Bayesian
 Information Criterion (BIC) (Burnham and Anderson, 2004). BIC penalizes more complex models ~~which~~
~~further, which~~ reduces the risk of overfitting. The distributed WB is then obtained by applying the resulting
~~regression coefficients to the topographic parameters associated with each gridecell. final set of β is then~~
 the weighted sum of β from all models. Distributed b_w is again calculated by multiplying the topographic
 parameters by the final set of β for all DEM gridcells.

~~Simple Ordinary~~ kriging

Simple kriging (SK) ~~is a data-driven~~ Kriging is a method of estimating dependent variables at unsampled
 locations by using the ~~isotropic spatial correlation (covariance)~~ spatial correlation of measured values to find a
 set of optimal weights (Davis and Sampson, 1986; Li and Heap, 2008). ~~Simple kriging~~ Kriging assumes spatial

correlation between ~~sampling locations that are~~ the dependent variables at the sampling locations distributed across a surface and then applies the correlation to interpolate between these locations. ~~We used the DiceKriging R package (Roustant and others, 2012) to calculate the maximum likelihood covariance matrix, as well as the range distance (θ) and nugget for gridcell-averaged values of winter balance. The range distance is a measure of data correlation length and the nugget is the residual that encompasses sampling error variance as well as the spatial variance at distances less than the minimum sample spacing (Li and Heap, 2008). Unlike topographic regression, simple kriging~~ Many forms of kriging have been developed to accommodate different data types (e.g. Li and Heap, 2008, and sources therein). Ordinary kriging (OK) is the simplest form of kriging in cases where the mean of the estimated field is unknown. Unlike LR, OK is not useful for generating hypotheses to explain the physical controls on snow distribution, nor can it be used to estimate winter balance on unmeasured glaciers. However, we chose to use OK because it does not require external inputs and is therefore a means of obtaining B_w that is free of physical interpretation beyond the information contained in the covariance matrix.

~~Uncertainty analysis~~

~~To quantify the uncertainty on estimates of glacier-wide WB we conduct a Monte Carlo analysis, which uses repeated random sampling of input variables to calculate a distribution of output variables (Metropolis and Ulam, 1949). We repeat the random sampling process 1000 times, resulting in a distribution of values of the glacier-wide WB based on uncertainties associated with~~ The OK model can be written $y(s) = \mu + z(s) + e$, where μ is the mean and e is independent white noise with standard deviation σ_e (also known as the nugget) that captures the sampling error as well as spatial variation at distances smaller than that observed in the sampling design (Li and Heap, 2008); $z(s)$ follows a mean-zero normal distribution with standard deviation σ_z . The covariance of observations at spatial locations s and s' is written as $Cov(z(s), z(s')) = \sigma_z^2 r(s, s')$ and r is a specified correlation model. We use the DiceKriging package in R (Roustant and others, 2012) to implement ordinary kriging. For our application we employ an isotropic Matérn correlation model with shape parameter $\nu = 5/2$ (see Rasmussen and Williams, 2006). This specification implies a fairly smooth response surface (twice differentiable) and is used in many applications (e.g. Stein, 1999). The model parameters, μ , σ_e , σ_z and range parameter for the Matérn correlation function are estimated using maximum likelihood. There is no closed form solution for these parameter estimates and they are found numerically. To ensure stability of the maximum likelihood solution, we use 500 random restarts of the ~~four steps outlined above. We use the standard deviation of this distribution as a useful~~

~~metric of uncertainty on the glacier-wide WB. DiceKringing~~ package (each with a different initial value of the parameters).

Uncertainty analysis using a Monte Carlo approach

Three sources of uncertainty are considered separately: the uncertainty due to (1) grid-scale variability of ~~WB~~ \tilde{b}_w (σ_{GS}), (2) the assignment of snow density (σ_ρ) and (3) interpolating and extrapolating gridcell-averaged values of ~~WB~~ \tilde{b}_w (σ_{INT}). ~~These individual~~ To quantify the combined uncertainty due to grid-scale variability, method of density assignment and interpolation uncertainty on estimates of B_w we conduct a Monte Carlo analysis that uses repeated random sampling of input variables to calculate a distribution of output variables (Metropolis and Ulam, 1949). We repeat the random sampling process 1000 times, resulting in a distribution of values of B_w based on uncertainties associated with the four steps we implement to derive B_w from distributed snow-depth and density measurements. Individual sources of uncertainty are propagated through the conversion of snow depth and density measurements to ~~glacier-wide WB~~ B_w . Finally, the combined effect of all three sources of uncertainty on ~~the glacier-wide WB~~ B_w is quantified. We ~~calculate~~ ~~a relative uncertainty as the normalized sum of differences between every pair of one hundred distributed WB estimates including~~ use the standard deviation of the distribution of B_w as a useful metric of B_w uncertainty. Density assignment uncertainty is calculated as the standard deviation of the eight resulting values of B_w . To investigate the spatial patterns in b_w uncertainty, we calculate a combined uncertainty, which is equal to the square root of the summed variance of distributed b_w that arises from σ_{GS} , σ_ρ and σ_{INT} . See Supplementary Material (Figs. S5 and S6) for plots of standard deviation of distributed b_w arising from individual sources of uncertainty.

Grid-scale uncertainty (σ_{GS})

We make use of the zigzag surveys to quantify the true variability of ~~WB~~ \tilde{b}_w at the grid scale. Our limited data do not permit a spatially-resolved assessment of grid-scale uncertainty, so we characterize this uncertainty as uniform across each glacier and represent it by a normal distribution. The distribution is centred at zero and has a standard deviation equal to the mean standard deviation of all zigzag measurements for each glacier. For each iteration of the Monte Carlo, ~~WB~~ \tilde{b}_w values are randomly chosen from the distribution and added to the values of gridcell-averaged ~~WB~~ \tilde{b}_w . These perturbed gridcell-averaged values of ~~WB~~ \tilde{b}_w are then used in the interpolation. We represent uncertainty in ~~glacier-wide WB~~ B_w due to grid-scale uncertainty (σ_{GS}) as the standard deviation of the resulting distribution of ~~glacier-wide WB~~ B_w estimates.

Density assignment uncertainty (σ_ρ)

We incorporate uncertainty due to the method of density assignment by carrying forward all eight density interpolation methods (Table 3) when estimating ~~glacier-wide WB~~ B_w . By choosing to retain even the least plausible options, as well as the questionable FS data, this approach results in a generous assessment of uncertainty. We represent the ~~glacier-wide WB~~ B_w uncertainty due to density assignment uncertainty (σ_ρ) as the standard deviation of ~~glacier-wide WB~~ B_w estimates calculated using each density assignment method.

Interpolation uncertainty (σ_{INT})

We represent the uncertainty due to interpolation/~~extrapolation~~ of gridcell-averaged ~~WB~~ b_w in different ways for LR and ~~SK~~OK. LR interpolation uncertainty is represented by a multivariate normal distribution of possible regression coefficients (~~β_i~~ β). The standard deviation of each distribution is calculated using the covariance of ~~regression coefficients~~ β as outlined in Bagos and Adam (2015), which ensures that ~~regression coefficients~~ the β values are internally consistent. The ~~β_i~~ β distributions are randomly sampled and used to calculate gridcell-estimated ~~WB~~ b_w .

~~SK~~OK interpolation uncertainty is represented by the ~~95% confidence interval for standard deviation for each~~ gridcell-estimated ~~values of WB value of~~ b_w generated by the DiceKriging package. ~~From this confidence interval, the standard deviation of each gridcell-estimated WB is then calculated.~~ The standard deviation of ~~glacier-wide WB~~ B_w is then found by taking the square root of the average variance of each gridcell-estimated ~~WB~~ b_w . The final distribution of ~~glacier-wide WB~~ B_w values is centred at the ~~glacier-wide WB estimated with SK~~ B_w estimated with OK. For simplicity, the standard deviation of ~~glacier-wide WB values that result~~ B_w values that results from either LR or ~~SK interpolation~~OK interpolation/~~extrapolation~~ uncertainty is referred to as σ_{INT} .

RESULTS AND DISCUSSION

Field measurements

Snow depth

Mean snow depth varied systematically across the study region, with Glacier 4 having the highest mean snow depth and Glacier 13 having the lowest (Fig. 2a). At each measurement location, the median range of measured depths (3–4 points) as a percent of the mean local depth is 2%, 11% and 12%, for Glaciers 4, 2 and 13, respectively. While Glacier 4 has the lowest point-scale variability, as assessed above, it also has the highest proportion of outliers, indicating a more variable snow depth across the glacier. The average

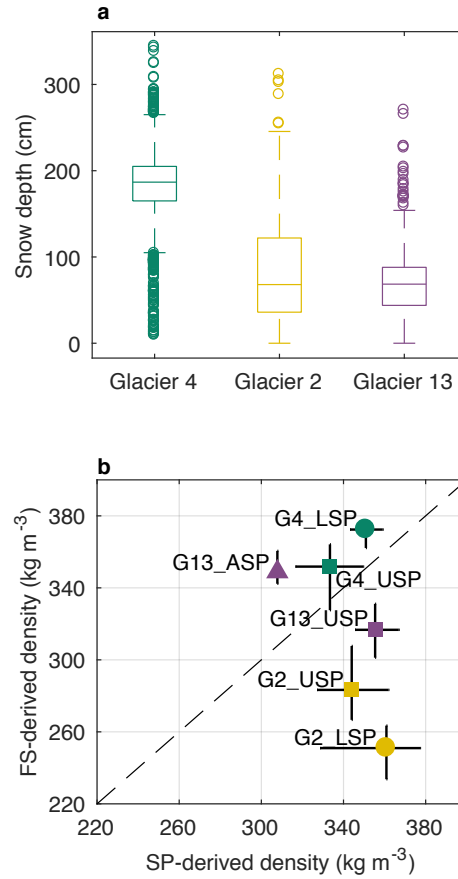


Fig. 2. Measured snow depth and density. (a) Boxplot of measured snow depth on Glaciers 4, 2 and 13 with the first quartiles (box), median (line within box), minimum and maximum values excluding outliers (bar) and outliers (circles), which are defined as being outside of the range of 1.5 times the quartiles (approximately $\pm 2.7\sigma$). (b) Comparison of depth-averaged densities estimated using Federal Sampler (FS) measurements and a wedge cutter in a snow pit (SP) for Glacier 4 (G4), Glacier 2 (G2) and Glacier 13 (G13). Labels indicate ~~snow-pit~~ SP locations in the accumulation area (ASP), upper ablation area (USP) and lower ablation area (LSP). Error bars for SP-derived densities are calculated by varying the thickness and density of layers that are too hard to sample, and error bars for FS-derived densities are the standard deviation of measurements taken at one location. One-to-one line is dashed.

standard deviation of all zigzag depth measurements is 0.07 m, 0.17 m and 0.14 m, for Glaciers 4, 2 and 13, respectively. When converted to values of ~~WB~~ b_w using the local FS-derived density measurement, the average standard deviation is 0.027 m w.e., 0.035 m w.e. and 0.040 m w.e. ~~WB~~ Winter-balance data for each zigzag are not normally distributed (Fig. 3).

~~Snow density~~

Contrary to expectation, co-located FS and SP measurements are found to be uncorrelated ($R^2 = 0.25$, Fig. 2b). The ~~Federal-Sampler~~ FS appears to oversample in deep snow and undersample in shallow snow.

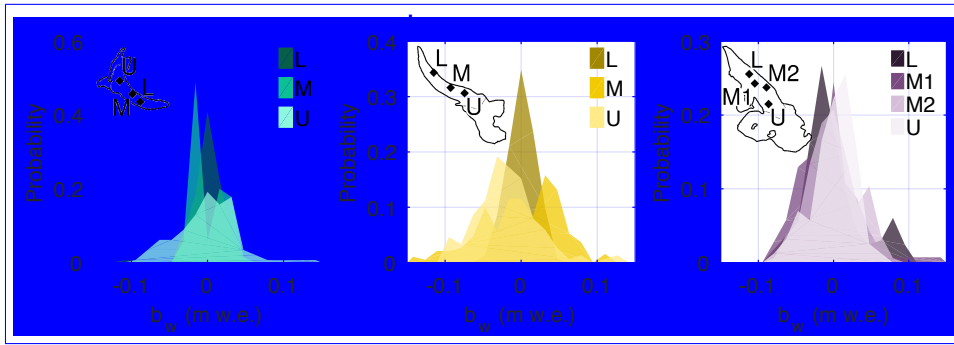


Fig. 3. Distributions of estimated winter-balance values for each zigzag survey in lower (L), middle (M) and upper (U) ablation areas (insets). Local mean has been subtracted. (a) Glacier 4. (b) Glacier 2. (c) Glacier 13.

Oversampling by small-diameter ~~(3.2–3.8 cm)~~ sampling tubes has been observed in previous studies, with a percent error between 6.8% and 11.8% (e.g. Work and others, 1965; Fames and others, 1982; Conger and McClung, 2009). Studies that use ~~Federal Samplers~~ FS often apply a 10% correction to all measurements for this reason (e.g. Molotch and others, 2005). Oversampling has been attributed to slots “shaving” snow into the tube as it is rotated (e.g. Dixon and Boon, 2012) and to snow falling into the slots, particularly for snow samples with densities $>400 \text{ kg m}^{-3}$ and snow depths $>1 \text{ m}$ (e.g. Beaumont and Work, 1963). Undersampling is likely to occur due to loss of snow from the bottom of the sampler (Turcan and Loijens, 1975). Loss by this mechanism may have occurred in our study, given the isothermal and melt-affected snow conditions observed over the lower reaches of Glaciers 2 and 13. Relatively poor ~~Federal Sampler~~ FS spring-scale sensitivity also calls into question the reliability of measurements for snow depths $<20 \text{ cm}$.

Our FS-derived density values are positively correlated with snow depth ($R^2 = 0.59$). This relationship could be a result of physical processes, such as compaction in deep snow and preferential formation of depth hoar in shallow snow, but is more likely a result of measurement artefacts for a number of reasons. First, the total range of densities measured by the ~~Federal Sampler~~ FS seems improbably large ($227\text{--}431 \text{ kg m}^{-3}$) ~~given the conditions at the~~. At the time of sampling, the snowpack had little new snow, few ice lenses and was not saturated; the range of measured densities is therefore difficult to explain with physical conditions. Moreover, the range of FS-derived values is much larger than ~~than that~~ of SP-derived values when co-located measurements are compared. Second, compaction effects of the magnitude required to explain the density differences between SP and FS measurements would not be expected at the measured snow depths (up to 340 cm). Third, no linear relationship exists between depth and SP-derived density ($R^2 = 0.05$). These findings suggest that the ~~Federal Sampler~~ FS measurements have a bias for which we have not identified a

suitable correction. [Despite this bias, we use FS-derived densities to generate a range of possible \$b_w\$ estimates and to provide a generous estimate of uncertainty arising from density assignment.](#)

Density assignment

Given the lack of correlation between co-located SP- and FS-derived densities (Fig. 2), we use the densities derived from these two methods separately (Table 3). SP-derived regional (S1) and glacier-mean (S2) densities are within one standard deviation of the corresponding FS-derived densities (F1 and F2) although SP-derived density values are larger (see Supplementary Material, Table [S2S3](#)). For both SP- and FS-derived densities, the mean density for any given glacier (S2 or F2) is within one standard deviation of the mean across all glaciers (S1 or F1). Correlations between elevation and SP- and FS-derived densities are generally high ($R^2 > 0.5$) but vary between glaciers (Supplementary ~~material, Table S2~~[Material, Table S3](#)). For any given glacier, the standard deviation of the 3–4 SP- or FS-derived densities is $<13\%$ of the mean of those values (S2 or F2) (Supplementary material, Table [S2S3](#)). We adopt S2 (glacier-wide mean of SP-derived densities) as the reference method of density assignment. Though the method described by S2 does not account for known basin-scale spatial variability in snow density (e.g. Wetlaufer and others, 2016), it is commonly used in winter balance studies (e.g. Elder and others, 1991; McGrath and others, 2015; Cullen and others, 2017).

Gridcell-averaged winter balance

The distributions of gridcell-averaged ~~WB- b_w~~ values for the individual glaciers are similar to those in Fig. 2a but with fewer outliers ~~–(see Supplementary Material, Fig. S4).~~ The standard deviations of ~~WB- b_w~~ values determined from the zigzag surveys are almost twice as large as the mean standard deviation of point-scale ~~WB- b_w~~ values within a gridcell measured along transects ~~–(see Supplementary Material, Fig. S5).~~ However, a small number of gridcells sampled in transect surveys have standard deviations in ~~WB- b_w~~ that exceed 0.25 m w.e. (~ 10 times greater than those for zigzag surveys). ~~We nevertheless assume that the gridecell uncertainty is captured with dense sampling in zigzag gridecells.~~

~~Distribution of coefficients (β_i) determined by linear regression of gridecell-averaged WB on DEM-derived topographic parameters for the eight different density assignment methods (Table 3). Coefficients are calculated using standardized data, so values can be compared across parameters. Regression coefficients that are not significant are assigned a value of zero. Topographic parameters include elevation (z), distance from centreline (d_C), slope (m), curvature (κ) and wind redistribution (Sx). Aspect (α) and “northness” (N) are not shown because coefficient values are zero in every case. The box plot shows first quartiles (box), median (line within box), mean (circle within box), minimum and maximum values excluding outliers~~

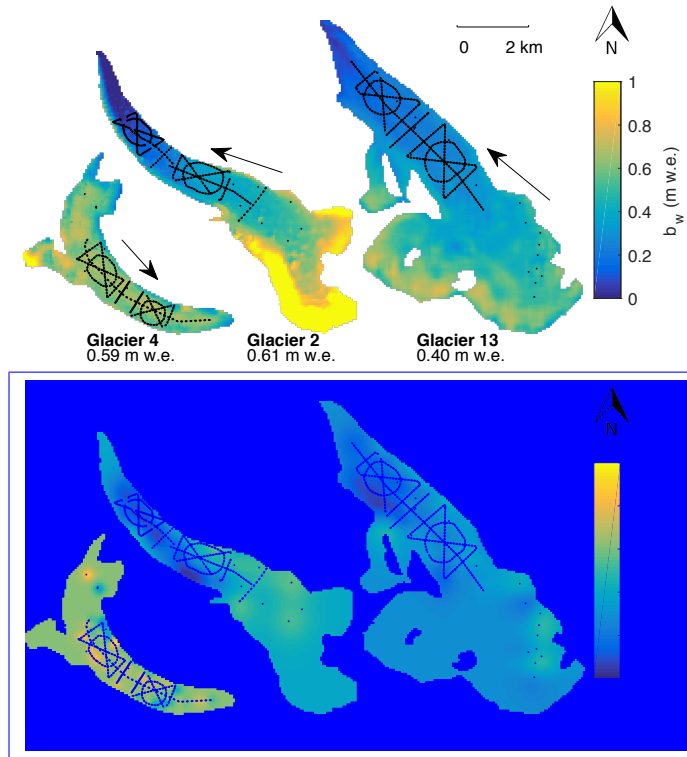


Fig. 4. Spatial distribution of winter balance (WB_{b_w}) estimated using linear regression (top row) and simple-ordinary kriging (bottom row) with densities assigned as per S2 (Table 3). The linear regression (LR) method involves multiplying regression coefficients, found using cross validation and model averaging, by topographic parameters for each gridcell. Ordinary kriging (OK) uses the correlation of measured values to find a set of optimal weights for estimating values at unmeasured locations. Locations of snow-depth measurements made in May 2016 are shown as black dots. Ice-flow directions are indicated by arrows. Values of glacier-wide-WB- B_w are given below labels.

(bars) and outliers (gray dots), which are defined as being outside of the range of 1.5 times the quartiles (approximately $\pm 2.7\sigma$).

Distributed winter balance

~~Distributed winter balance~~

Relative uncertainty in distributed winter balance (WB) (Fig. 4) found using linear regression (top row) and simple kriging (bottom row). Values closer to one indicate higher relative uncertainty. Ice-flow directions are indicated by arrows.

Linear regression

The highest values of estimated b_w are found in the upper portions of the accumulation areas of Glaciers 2 and 13 (Fig. 4). These areas also correspond to large values of elevation, slope, and wind redistribution.

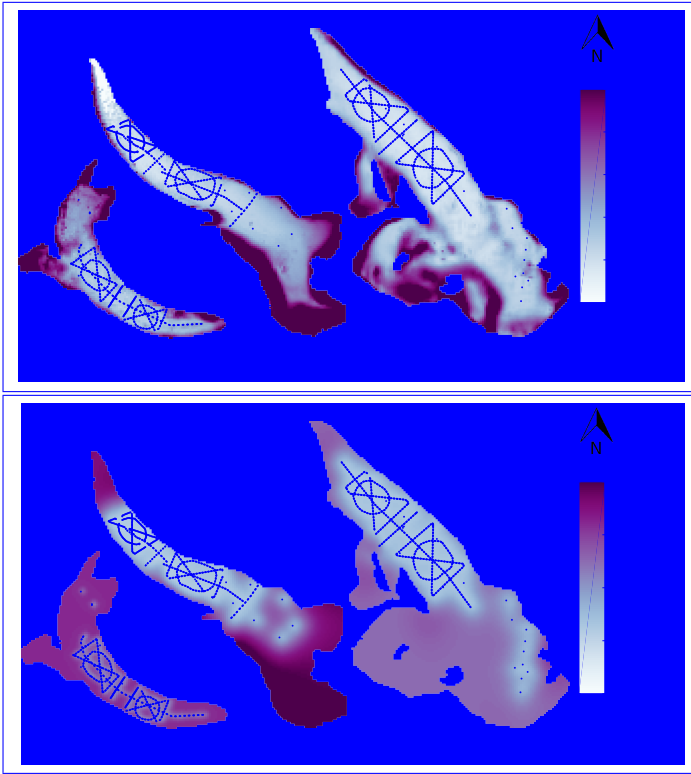


Fig. 5. Combined uncertainty of distributed winter balance (b_w) for density-assignment method S2 (Fig. 4) found using linear regression (top row) and ordinary kriging (bottom row). Ice-flow directions are indicated by arrows.

Extrapolation of the positive relation between b_w and elevation, as well as slope and Sx for Glacier 2, results in high b_w estimates and large combined uncertainty in these estimates (Fig. 5). On Glacier 4, the distributed b_w is nearly uniform (Fig. 4) due to the small regression coefficients for all topographic parameters. The variance explained by the LR-estimated b_w differs considerably between glaciers (Fig. 6), with the best correlation

Table 4. Glacier-wide winter balance (WB_{B_w} , m w.e.) estimated using linear regression and simple ordinary kriging for the three study glaciers. Root mean squared error (RMSE, m w.e.) is computed as the average of all RMSE values between gridcell-averaged values of WB_{B_w} (the data) that were randomly selected and excluded from interpolation ($1/3 \sim 1/3$ of all data) and those estimated by interpolation. RMSE as a percent of the glacier-wide WB_{B_w} is shown in brackets/parentheses.

	Linear regression		Ordinary kriging	
	WB_{B_w}	RMSE	WB_{B_w}	RMSE
G4	0.58	0.15 (26%)	0.62	0.13 (21) 0.11 (18%)
G2	0.58	0.10 (17%)	0.37 0.35	0.07 (19) 0.06 (18%)
G13	0.38	0.08 (21%)	0.27	0.07 (26) 0.06 (21%)

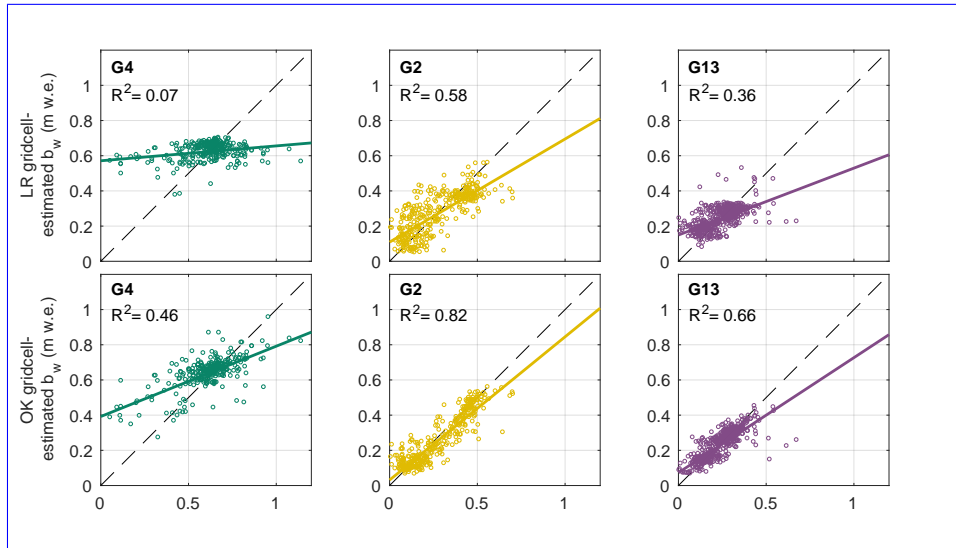


Fig. 6. Winter balance (b_w) estimated by linear regression (LR, top row) or ordinary kriging (OK, bottom row) versus the grid-cell averaged b_w data for Glacier 4 (left), Glacier 2 (middle) and Glacier 13 (right). Each circle represents a single gridcell. Explained variance (R^2) is provided. Best-fit (solid) and one-to-one (dashed) lines are shown.

between modelled and observed b_w occurring for Glacier 2. LR is an especially poor predictor of b_w on Glacier 4, where B_w can be estimated equally well using the mean of the data. RMSE is also highest for Glacier 4 (Table 4).

Ordinary kriging

For all three glaciers, large areas that correspond to locations far from measurements have b_w estimates equal to the kriging mean. Distributed b_w estimated with OK on Glacier 4 is mostly uniform except for local deviations close to measurement locations (Fig. 4) and combined uncertainty is high across the glacier. Distributed b_w varies more smoothly on Glaciers 2 and 13 (Fig. 4). Glacier 2 has a distinct region of low estimated b_w (~ 0.1 m w.e.) in the lower part of the ablation area, which corresponds to a wind-scoured region of the glacier. Glacier 13 has the lowest estimated mean b_w and only small deviations from this mean at measurement locations (Fig. 4). Combined uncertainty varies considerably across the three study glaciers with the greatest uncertainty far from measurement locations (Fig. 5). The variance explained by OK-estimated b_w is high for Glaciers 2 and 13 relative to that for Glacier 4 (Fig. 6).

Uncertainty analysis using a Monte Carlo approach

Linear Regression

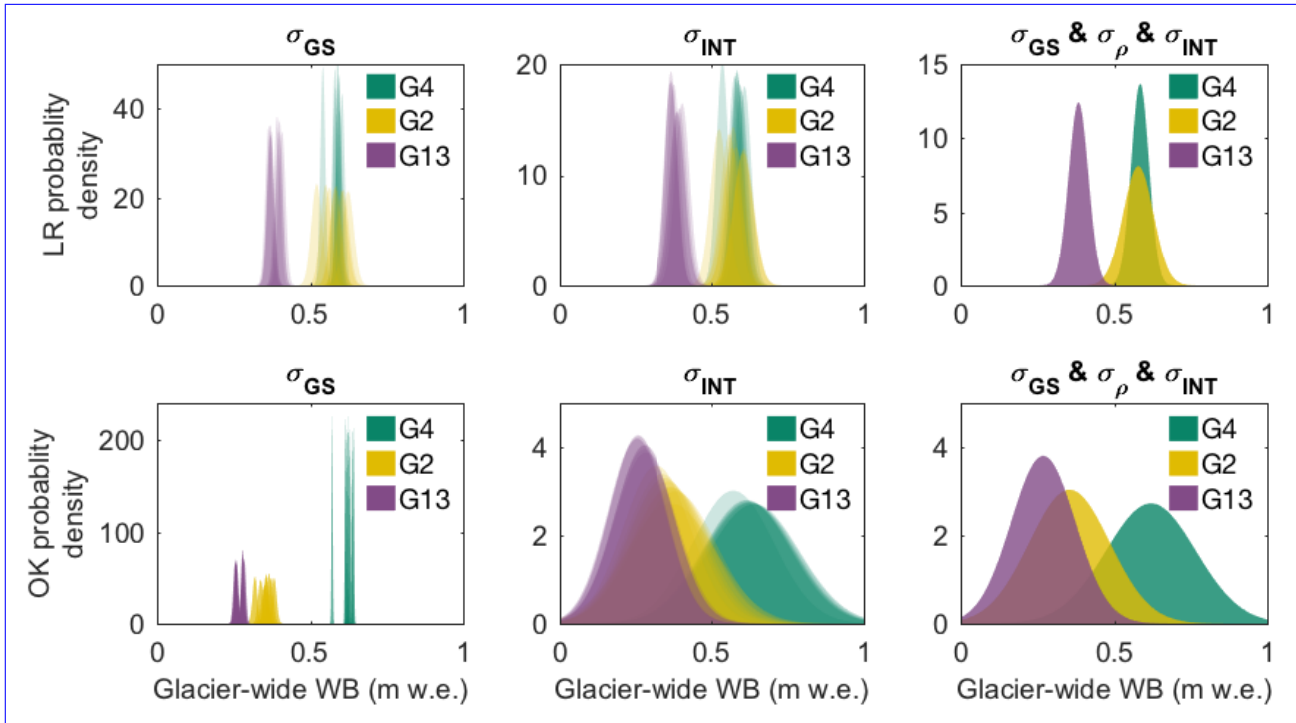


Fig. 7. Winter Distributions of glacier-wide winter balance (B_w) estimated by linear regression for Glaciers 4 (LRG4), top row 2 (G2) or simple kriging and 13 (SK, bottom row G13) versus the grid-cell averaged WB data for Glacier 4 that arise from various sources of uncertainty. B_w distribution arising from grid-scale uncertainty (σ_{GS}) (left column); Glacier 2, B_w distribution arising from interpolation uncertainty (σ_{INT}) (middle column). B_w distribution arising from a combination of σ_{GS} , σ_{INT} and Glacier 13 density assignment uncertainty (σ_ρ) (right column). Each circle represents a single gridcell. Results are shown for interpolation by linear regression (LR, top row) and ordinary kriging (OK, bottom row). Best-fit Left two columns include eight distributions per glacier (solid colour) and one-to-one each corresponds to a density assignment method (dashed S1–S4 and F1–F4) lines are shown.

472 Estimates of B_w are affected by uncertainty introduced by the representativeness of gridcell-averaged values of
 473 b_w (σ_{GS}), choosing a method of density assignment (σ_ρ), and interpolating/extrapolating b_w values across the
 474 domain (σ_{INT}). Using a Monte Carlo analysis, we find that interpolation uncertainty contributes more to B_w
 475 uncertainty than grid-scale uncertainty or the method of density assignment (see Supplementary Material). In
 476 other words, the distribution of B_w that arises from grid-scale uncertainty and the differences in distributions
 477 of B_w due to different methods of density assignment are generally smaller than the distribution that arises
 478 from interpolation uncertainty (Fig. 7 and Table 5). The B_w distributions obtained using LR and OK overlap
 479 for a given glacier, but the distribution modes differ (Fig. 7). OK-estimated values of b_w in the accumulation
 480 area are generally lower (Fig. 4), which lowers the B_w estimate. The uncertainty in OK-estimated values of
 481 B_w is large, and unrealistic values (e.g. $B_w = 0$ m w.e.) are possible (Fig. 7).

Table 5. Standard deviation ($\times 10^{-2}$ m w.e.) of glacier-wide winter balance (B_w) distributions arising from uncertainties in grid-scale b_w (σ_{GS}), density assignment (σ_ρ), interpolation (σ_{INT}) and all three sources combined (σ_{ALL}) for linear regression (left columns) and ordinary kriging (right columns)

	Linear regression				Ordinary kriging			
	σ_{GS}	σ_ρ	σ_{INT}	σ_{ALL}	σ_{GS}	σ_ρ	σ_{INT}	σ_{ALL}
Glacier 4	0.86	1.90	2.13	2.90	0.18	2.16	14.35	14.64
Glacier 2	1.80	3.37	3.09	4.90	0.80	2.06	12.65	13.14
Glacier 13	1.12	1.68	2.80	3.20	0.57	1.30	9.74	10.48

The values of B_w for our study glaciers (using LR and the S2 density assignment), with an uncertainty equal to one standard deviation of the distribution found with Monte Carlo analysis, are: 0.59 ± 0.03 m w.e. for Glacier 4, 0.61 ± 0.05 m w.e. for Glacier 2 and 0.40 ± 0.03 m w.e. for Glacier 13. The B_w uncertainty from the three investigated sources of uncertainty ranges from 0.03 m w.e (5%) to 0.05 m w.e (8%) for LR estimates and from 0.10 m w.e (37%) to 0.15 m w.e (24%) for ordinary-kriging estimates.

DISCUSSION

Distributed winter balance

Linear regression

Of the topographic parameters in the ~~linear regression~~LR, elevation (z) is the most significant predictor of gridcell-averaged ~~WB~~ b_w for Glaciers 2 and 13, while wind redistribution (Sx) is the most significant predictor for Glacier 4 (Fig. 8, ~~Fig. 4~~). As expected, gridcell-averaged ~~WB~~ b_w is positively correlated with elevation where the correlation is significant. It is possible that the elevation correlation was accentuated due to melt onset for Glacier 13 in particular. ~~Many studies~~ Glacier 2 had little snow at the terminus likely due to steep slopes and wind-scouring but the snow did not appear to have been affected by melt. Our results are consistent with many studies that have found elevation to be the most significant predictor of ~~winter-balance data (e.g. Machguth and others, 2006; McGrath and others, 2015).~~ However, ~~WB~~ elevation gradients vary considerably between glaciers (e.g. Winther and others, 1998) and other factors, such as glacier shape and orientation relative to dominant wind direction, are strong predictors of the ~~winter-balance distribution (Machguth and others, 2006; Grabiec and others, 2011).~~ Some studies find no significant correlation between ~~WB~~ on glaciers and topographic parameters, with ~~seasonal snow accumulation data~~ (e.g. Machguth and others, 2006; Grünewald and others, 2014; McGrath and others, 2015). The

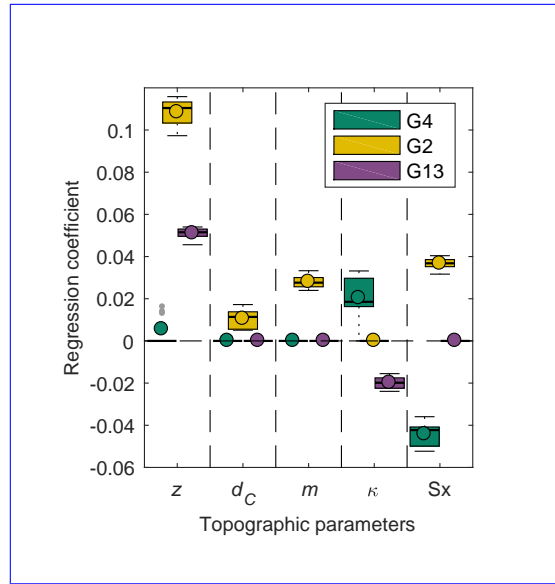


Fig. 8. Distribution of coefficients (β) determined by linear regression of gridcell-averaged b_w on DEM-derived topographic parameters for the eight different density assignment methods (Table 3). Coefficients are calculated using standardized data, so values can be compared across parameters. Regression coefficients that are not significant are assigned a value of zero. Topographic parameters include elevation (z), distance from centreline (d_C), slope (m), curvature (κ) and wind redistribution (Sx). Aspect (α) and “northness” (N) are not shown because coefficient values are zero in every case. The box plot shows first quartiles (box), median (line within box), mean (circle within box), minimum and maximum values excluding outliers (bars) and outliers (gray dots), which are defined as being outside of the range of 1.5 times the quartiles (approximately $\pm 2.7\sigma$).

b_w -elevation gradient is $13 \text{ mm } 100 \text{ m}^{-1}$ on Glacier 2 and $7 \text{ mm } 100 \text{ m}^{-1}$ on Glacier 13. These gradients are consistent with those reported for a few glaciers in Svalbard (Winther and others, 1998) but are considerably smaller than many reported b_w -elevation gradients, which range from about 60 to $240 \text{ mm } 100 \text{ m}^{-1}$ (e.g. Hagen and Liestøl, 1990; Tveit and Killingtveit, 1994; Winther and others, 1998). Extrapolating linear relationships to unmeasured locations typically results in considerable estimation error, as seen by the large b_w values (Fig. 4) and large combined uncertainty (Fig. 5) in the high-elevation regions of Glaciers 2 and 13. The low correlation between b_w and elevation on Glacier 4 is consistent with Grabiec and others (2011) and López-Moreno and others (2011), who conclude that highly variable distributions of snow can be attributed to complex interactions between topography and the atmosphere that could not be easily quantified (e.g. Grabiec and others, 2011; López-Moreno and others, 2011). Extrapolating relationships to unmeasured locations, especially the accumulation area, is susceptible to large uncertainties (Fig. 5). This extrapolation has a considerable effect on values of glacier-wide WB, as the highest values of WB are

typically found in the accumulation area (Fig. 4). The snow on Glacier 4 also did not appear to have been affected by melt and it is hypothesized that significant wind-redistribution of snow, which was not captured by the Sx parameter, covered ice-topography and produced a relatively uniform snow depth across the glacier.

Gridcell-averaged $WB - b_w$ is negatively correlated with Sx on Glacier 4, counter-intuitively indicating less snow in what would be interpreted as sheltered areas. Gridcell-averaged $WB - b_w$ is positively correlated with Sx on Glaciers 2 and 13. Similarly, gridecell-averaged WB is positively correlated with curvature on Glacier 4 and negatively correlated on Glaciers 2 and 13. Wind redistribution and preferential deposition of snow are known to have a large influence on snow distribution at sub-basin scales (e.g. Dadić and others, 2010; Winstral and others, 2013; Gerber and others, 2017). Our results corroborate those of McGrath and others (2015) in a study of six glaciers in Alaska (DEM resolutions of 5 m) where elevation and Sx were the only significant parameters for all glaciers; Sx regression coefficients were smaller than elevation regression coefficients, and in some cases, negative. While our results point to wind having an impact on snow distribution, but the wind redistribution parameter (Sx) may not adequately capture these effects at our study sites. For example, Glacier 4 is located in a curved valley with steep side walls, so specifying a single cardinal direction for wind may not be adequate. Further, the scale of deposition may be smaller than the resolution of the Sx parameter estimated from the DEM. Our results corroborate those of McGrath and others (2015) in a study of six glaciers in Alaska (DEM resolutions of 5 m) where elevation and Sx were the only significant parameters for all glaciers; Sx regression coefficients were smaller than elevation regression coefficients, and in some cases, negative. In addition to wind redistribution, Creation of a parametrization for sublimation from blowing snow has also, which has been shown to be an important mechanism of mass loss from ridges (e.g. Musselman and others, 2015). Incorporating such losses, as well as redistribution and preferential deposition, may be important for improving representations of distributed winter balance, may also increase the explanatory power of LR for our study sites.

We find that transfer of LR coefficients between glaciers results in large estimation errors. Regression coefficients from Glacier 4 produce the highest root-mean-squared-error RMSE (0.38 m w.e. on Glacier 2 and 0.40 m w.e. on Glacier 13, see Table 4 for comparison) and glacier-wide $WB - B_w$ values are the same for all glaciers (0.64 m w.e.) due to the dominance of the regression intercept. Even if the regression LR is performed with $WB - b_w$ values from all glaciers combined, the resulting coefficients produce large root-mean-squared

errors RMSE when applied to individual glaciers (0.31 m w.e., 0.15 m w.e. and 0.14 m w.e. for Glaciers 4, 2 and 13, respectively). Our results are consistent with those of Grünwald and others (2013), who found that local statistical models cannot be transferred across basins and that regional-scale models are not able to explain the majority of observed variance in winter balance.

~~Simple Ordinary~~ kriging

~~Fitted kriging parameters, including the nugget and spatial correlation length, can provide insight into important scales of winter balance variability. The model fitted to the gridcell-averaged values of WB for Glacier 4 has a short correlation length (90 m) and large nugget (see Supplementary Material Table S3), suggesting variability in winter balance at smaller scales. Conversely, Glaciers 2 and 13 have longer correlation lengths (~450 m) and smaller nuggets, suggesting variability at larger scales. Additionally, simple kriging is better able to estimate values of WB for Glaciers 2 and 13 than for Glacier 4 (Fig. 6). Due to a paucity of data, simple ordinary kriging produces almost uniform gridcell-estimated values of winter balance b_w in the accumulation area of each glacier, inconsistent with observations described in the literature (e.g. Machguth and others, 2006; Grabiec and others, 2011). Extrapolation using simple kriging Glacier 4 has the highest estimated mean with large deviations from the mean at measurement locations. The longer correlation lengths of the data for Glaciers 2 and 13 result in a more smoothly varying distributed b_w . As expected, extrapolation using OK leads to large uncertainty (Fig. 5), further emphasizing the need for spatially distributed point-scale measurements.~~

LR and ~~SK-OK~~ comparison

~~Glacier-wide WB estimates found using both LR and SK are LR and OK produce similar estimates of distributed b_w (Fig. 4) and B_w (~0.580.60 m w.e., Table 4) for Glacier 4 but both are relatively poor predictors of WB b_w in measured gridcells (Table 4 Fig. 6). For Glaciers 2 and 13, SK-OK estimates are more than 0.1~0.22 m w.e. (up to 40%)~39% and ~0.11 m w.e. (30%) lower than LR estimates, respectively (Table 4). RMSE as a percentage of the B_w is lower for OK than LR only for Glacier 4 but the absolute RMSE of OK is ~0.03 m w.e. lower for all glaciers, likely because OK is a data-fitting interpolation method (Table 4). RMSEs as a percentage of glacier-wide WB B_w are comparable between LR and SK-OK (Table 4) with an average RMSE of 22%. This comparability is interesting, given that all of the data were used to generate the SK-OK model, while only 2/3~2/3 were used in the LR. Tests in which only ~2/3 of the data were used in the OK model yielded similar results to those in which all data were used. Gridcell-estimated values of WB b_w found using LR and SK-OK differ markedly in the upper accumulation areas of Glaciers 2 and 13 (Fig.~~

4), where observations are sparse and topographic parameters, such as elevation, ~~vary considerably~~ attain
their highest values. The influence of elevation results in substantially higher LR-estimated values of ~~WB~~ b_w
at high elevation, whereas ~~SK-estimated values approximate the nearest data~~ OK-estimated values are more
uniform. Estimates of ablation-area-wide ~~WB~~ B_w differ by ~~<76%~~ between LR and ~~SK~~ OK on each glacier,
further emphasizing the combined ~~role~~ influence of interpolation method and measurement scarcity in the
accumulation area on ~~glacier-wide WB~~ B_w estimates.

~~Distributions of glacier-wide winter balance (WB) for Glaciers 4 (G4), 2 (G2) and 13 (G13) that arise from~~
~~various sources of uncertainty. WB distribution arising from grid-scale uncertainty (σ_{GS}) (left column). WB~~
~~distribution arising from interpolation uncertainty (σ_{INT}) (middle column). WB distribution arising from~~
~~a combination of σ_{GS} , σ_{INT} and density assignment uncertainty (σ_ρ) (right column). Results are shown for~~
~~interpolation by linear regression (LR, top row) and simple kriging (SK, bottom row). Left two columns~~
~~include eight distributions per glacier (colour) and each corresponds to a density assignment method (S1–S4~~
~~and F1–F4).~~

Uncertainty analysis using a Monte Carlo approach

~~Uncertainty analysis~~

~~Glacier-wide winter balance is affected by uncertainty introduced by the representativeness of~~
~~gridecell-averaged values of WB (σ_{GS}), choosing a method of density assignment (σ_ρ), and interpolating~~
~~WB values across the domain (σ_{INT}). Using a Monte Carlo analysis, we find that interpolation uncertainty~~
~~contributes more to WB uncertainty than grid-scale uncertainty or density assignment method. In other~~
~~words, the distribution of glacier-wide WB that arises from grid-scale uncertainty and the differences in~~
~~distributions between methods of density assignment are smaller than the distribution that arises from~~
~~interpolation uncertainty (Fig. 7 and Table 5). The WB distributions obtained using LR and SK overlap~~
~~for a given glacier, but the distribution modes differ (Fig. 7). For reasons outlined above, SK-estimated~~
~~values of WB in the accumulation area are generally lower, which lowers the glacier-wide WB estimate. The~~
~~uncertainty in SK-estimated values of WB is large, and unrealistic glacier-wide values of WB of 0 m w.e. can~~
~~be estimated (Fig. 7). Our~~ Interpolation/extrapolation of b_w data is the largest contributor to b_w uncertainty
in our study. These results caution strongly against including interpolated/extrapolated values of ~~WB~~ b_w in
comparisons with remote sensing- or model-derived estimates of ~~WB~~ b_w . If possible, such comparisons should
be restricted to point-scale data.

Standard deviation ($\times 10^{-2}$ m w.e.) of glacier-wide winter balance distributions arising from uncertainties in grid-scale WB (σ_{GS}), density assignment (σ_{ρ}), interpolation (σ_{INT}) and all three sources combined (σ_{ALL}) for linear regression (left columns) and simple kriging (right columns) σ_{GS} σ_{ρ} σ_{INT} σ_{ALL} σ_{GS} σ_{ρ} σ_{INT} σ_{ALL}

~~Glacier 4~~ 0.86 1.90 2.13 2.90 0.85 2.15 14.05 14.72 ~~Glacier 2~~ 1.80 3.37 3.09 4.90 2.53 2.03 13.78 13.44

~~Glacier 13~~ 1.12 1.68 2.80 3.20 1.15 1.27 9.65 10.43

Grid-scale uncertainty (σ_{GS}) is the smallest assessed contributor to overall ~~WB~~ B_w uncertainty. This result is consistent with the generally smoothly-varying snow depths encountered in zigzag surveys, and previously reported ice-roughness lengths on the order of centimetres (e.g. Hock, 2005) compared to snow depths on the order of decimetres to metres. Given our assumption that zigzags are an adequate representation of grid-scale variability, the low ~~WB~~ B_w uncertainty arising from σ_{GS} implies that subgrid-scale sampling need not be a high priority for reducing overall uncertainty. Our assumption that the 3–4 zigzag surveys can be used to estimate glacier-wide σ_{GS} may be flawed, particularly in areas with debris cover, crevasses and steep slopes.

Our analysis did not include uncertainty arising from ~~a number of sources, which we assume either to be encompassed by the sources investigated or to be negligible contributors. These sources of uncertainty include~~ density measurement errors associated with the ~~Federal Sampler~~ FS , wedge cutters and spring scales, ~~from~~ vertical and horizontal errors in the DEM ~~and or from~~ error associated with estimating measurement locations –

The values of glacier-wide WB for our study glaciers (using LR and S2 density assignment method), with ~~an uncertainty equal to one standard deviation of the distribution found with Monte Carlo analysis, are:~~ 0.59 ± 0.03 m w.e. for Glacier 4, 0.61 ± 0.05 m w.e. for Glacier 2 and 0.40 ± 0.03 m w.e. for Glacier 13. The ~~glacier-wide WB uncertainty from combined~~ based on the GPS position of the lead observer. We assume that these sources of uncertainty ~~ranges from 0.03 m w.e (5%) to 0.05 m w.e (8%) for linear regression estimates and from 0.10 m w.e (37%) to 0.15 m w.e (24%) for simple kriging estimates (Table 4). are either encompassed by the sources investigated or are negligible.~~

~~Context and caveats~~ Regional winter-balance gradient

~~Regional winter-balance gradient~~

Although we find considerable inter- and intra-basin variability in winter balance, our results are consistent with a regional-scale winter-balance gradient for the continental side of the St. Elias Mountains (Fig. 9). Winter-balance data are compiled from Taylor-Barge (1969), the three glaciers presented in this paper and two ~~snow pits~~ SP we analyzed near the head of the Kaskawulsh Glacier between 20–21 May 2016. The

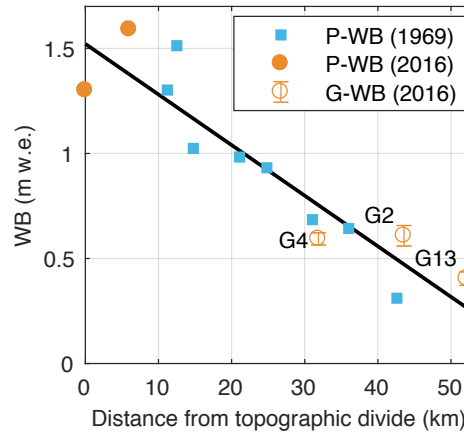


Fig. 9. Relationship between winter balance (WB) and linear distance from the regional topographic divide between the Kaskawulsh and Hubbard Glaciers in the St. Elias Mountains. Point-scale values of WB-winter balance from snow-pit data reported by Taylor-Barge (1969) (blue boxes, P-WB). LR-estimated glacier-wide WB-winter balance (B_w) calculated using density assignment S2 for Glaciers 4 (G4), 2 (G2) and 13 (G13) with errors bars calculated as the standard deviation of Monte Carlo-derived WB- B_w distributions (this study) (open orange circles, G-WB). Point-scale WB-winter balance estimated from snow-pit data at two locations in the accumulation area of the Kaskawulsh Glacier, collected in May 2016 (unpublished data, SFU Glaciology Group) (filled orange dots, P-WB). Black line indicates best fit ($R^2 = 0.85$).

data show a linear decrease of $0.024 \text{ m.w.e. km}^{-1}$ ($R^2 = 0.85$) in winter balance with distance from the regional topographic divide between the Kaskawulsh and Hubbard Glaciers, as identified by Taylor-Barge (1969). While the three study glaciers fit the regional trend, the same relationship would not apply if just the Donjek Range were considered. We hypothesize that interaction between meso-scale weather patterns and large-scale mountain topography is a major driver of regional-scale winter balance. Further insight into regional-scale patterns of winter balance in the St. Elias Mountains could be gained by investigating moisture source trajectories and the contribution of orographic precipitation.

~~Limitations and future work~~

Limitations and future work

The potential limitations of our work include the restriction of our data to a single year, minimal sampling in the accumulation area, the problem of uncorrelated SP- and FS-derived densities, a sampling design that could not be optimized ~~a-priori~~ a-priori, the assumption of spatially uniform subgrid variability and lack of more finely resolved DEMs.

647 Inter-annual variability in winter balance is not considered in our study. A number of studies have found
648 temporal stability in spatial patterns of snow distribution and that statistical models based on topographic
649 parameters could be applied reliably between years (e.g. Grünewald and others, 2013). For example, Walmsley
650 (2015) analyzed more than 40 years of winter balance recorded on two Norwegian glaciers and found that
651 snow distribution is spatially heterogeneous yet exhibits robust temporal stability. Contrary to this, Crochet
652 and others (2007) found that snow distribution in Iceland differed considerably between years and depended
653 primarily on the dominant wind direction over the course of a winter. Therefore, multiple years of snow depth
654 and density measurements, that are not necessarily consecutive, are needed to better understand inter-annual
655 variability ~~in-winter-balance-distribution~~ of winter balance within the Donjek Range.

656 There is a conspicuous lack of data in the accumulation areas of our study glaciers. With increased sampling
657 in the accumulation area, interpolation uncertainties would be reduced where they are currently greatest
658 and the ~~linear regression~~ LR would be better constrained. Although certain regions of the glaciers remain
659 inaccessible for direct measurements, other methods of obtaining winter-balance measurements, including
660 ground-penetrating radar and DEM differencing with photogrammetry or lidar, could be used in conjunction
661 with manual probing to increase the spatial coverage of measurements.

662 The lack of correlation between SP- and FS-derived densities needs to be reconciled. Contrary to our
663 results, most studies that compare SP- and FS-derived densities report minimal discrepancy (e.g. Dixon
664 and Boon, 2012, and sources within). Additional co-located density measurements are needed to better
665 compare the two methods of obtaining density values. Comparison with other ~~Federal Samplers~~ FS would
666 also be informative. Even with this limitation, density assignment was, fortunately, not the largest source of
667 uncertainty in estimating glacier-wide winter balance.

668 Our sampling design was chosen to achieve broad spatial coverage of the ablation area, but is likely too
669 finely resolved along transects for many mass-balance surveys to replicate. An optimal sampling design would
670 minimize uncertainty in winter balance while reducing the number of required measurements. Analysis of
671 the estimated winter balance obtained using subsets of the data is underway to make recommendations on
672 optimal transect configuration and along-track spacing of measurements. López-Moreno and others (2010)
673 found that 200–400 observations are needed within a non-glacierized alpine basin (6 km²) to obtain accurate
674 and robust snow distribution models. Similar guidelines would be useful for glacierized environments.

675 In this study, we assume that the subgrid variability of winter balance is uniform across a given glacier.
676 Contrary to this assumption, McGrath and others (2015) found greater variability of winter-balance values

close to the terminus. Testing our assumption could be a simple matter of prioritizing the labour-intensive zigzags surveys. To ensure consistent quantification of subgrid variability, zigzag survey measurements could also be tested against other measurements methods, such as lidar.

DEM gridcell size is known to influence values of computed topographic parameters (Zhang and Montgomery, 1994; Garbrecht and Martz, 1994; Guo-an and others, 2001; López-Moreno and others, 2010). The relationship between topographic parameters and winter balance is, therefore, not independent of DEM gridcell size. For example, Kienzle (2004) and López-Moreno and others (2010) found that a decrease in spatial resolution of the DEM results in a decrease in the importance of curvature and an increase in the importance of elevation in ~~regressions~~-LR of snow distribution on topographic parameters in non-glacierized basins. The importance of curvature in our study is affected by the DEM smoothing that we applied to obtain a spatially continuous curvature field (see Supplementary Material, Fig. S1). A comparison of regression coefficients from high-resolution DEMs obtained from various sources and sampled with various gridcell sizes could be used to characterize the dependence of topographic parameters on DEMs, and therefore assess the robustness of inferred relationships between winter balance and topographic parameters.

CONCLUSION

We estimate winter balance for three glaciers (termed Glacier 2, Glacier 4 and Glacier 13) in the St. Elias Mountains, Yukon, Canada from multiscale snow depth and density measurements. Linear regression and ~~simple-ordinary~~ kriging are used to obtain estimates of distributed winter balance (b_w). We use Monte Carlo analysis to evaluate the contributions of interpolation, ~~the~~ assignment of snow density and grid-scale variability of winter balance to uncertainty in estimates of glacier-wide winter balance (B_w).

Values of ~~glacier-wide winter balance~~- B_w estimated using linear regression and ~~simple-ordinary~~ kriging differ by up to 0.24 m w.e. ($\sim 50\%$). We find that interpolation uncertainty is the largest assessed source of uncertainty in ~~glacier-wide winter balance~~- B_w (7% for linear-regression estimates and ~~32% for simple-kriging~~ 34% for ordinary-kriging estimates). Uncertainty resulting from the method of density assignment is comparatively low, despite the wide range of methods explored. Given our representation of grid-scale variability, the resulting ~~winter balance~~- B_w uncertainty is small indicating that extensive subgrid-scale sampling is not required to reduce overall uncertainty.

Our results suggest that processes governing distributed ~~winter balance~~- b_w differ between glaciers, highlighting the importance of regional-scale winter-balance studies. The estimated distribution of ~~winter balance~~- b_w on Glacier 4 is characterized by high variability, as indicated by the poor correlation between

estimated and observed values and large number of data outliers. Glaciers 2 and 13 appear to have lower spatial variability, with elevation being the dominant predictor of gridcell-averaged ~~winter-balance~~ b_w . A wind-redistribution parameter is found to be a weak but significant predictor of ~~winter-balance~~ b_w , though conflicting relationships between glaciers make it difficult to interpret. The major limitations of our work include the restriction of our data to a single year and minimal sampling in the accumulation area. Although challenges persist when estimating winter balance, our data are consistent with a regional-scale winter-balance gradient for the continental side of the St. Elias Mountains.

AUTHOR CONTRIBUTION STATEMENT

AP planned and executed the data collection, performed all calculations and ~~drafted-analysis and drafted~~ and edited the manuscript. GF conceived of the study, contributed to field planning and data collection, oversaw all stages of the work and edited the manuscript. VR provided guidance ~~with-statistical-methods~~ on the methods of data analysis and edited the manuscript. DB provided insight into the statistical analysis and edited the manuscript.

ACKNOWLEDGEMENTS

We thank the Kluane First Nation (KFN), Parks Canada and the Yukon Territorial Government for granting us permission to work in KFN Traditional Territory and Kluane National Park and Reserve. We are grateful for financial support provided by the Natural Sciences and Engineering Research Council of Canada, Simon Fraser University and the Northern Scientific Training Program. We kindly acknowledge Kluane Lake Research Station, Sian Williams, Lance Goodwin and Trans North pilot Dion Parker for facilitating field logistics. We are grateful to Alison Criscitiello and Coline Ariagno for all aspects of field assistance and Sarah Furney for assistance with data entry. Thank you to Etienne Berthier for providing us with the SPIRIT SPOT-5 DEM and for assistance in DEM correction. We are grateful to ~~Derek-Bingham and~~ Michael Grosskopf for assistance with the statistics, including ~~simple-ordinary~~ kriging. Luke Wonneck, Leif Anderson and Jeff Crompton all provided thoughtful and constructive comments on drafts of the manuscript. We appreciate the thoughtful suggestions and edits from two anonymous reviewers.

REFERENCES

Anderton S, White S and Alvera B (2004) Evaluation of spatial variability in snow water equivalent for a high mountain catchment. *Hydrological Processes*, **18**(3), 435–453 (doi: 10.1002/hyp.1319)

- 735 Arendt AA, Luthcke SB, Larsen CF, Abdalati W, Krabill WB and Beedle MJ (2008) Validation of high-resolution
736 GRACE mascon estimates of glacier mass changes in the St Elias Mountains, Alaska, USA, using aircraft laser
737 altimetry. *Journal of Glaciology*, **54**(188), 778–787 (doi: 10.3189/002214308787780067)
- 738 Bagos PG and Adam M (2015) On the Covariance of Regression Coefficients. *Open Journal of Statistics*, **5**, 680–701
739 (doi: 10.4236/ojs.2015.57069)
- 740 Balk B and Elder K (2000) Combining binary decision tree and geostatistical methods to estimate snow distribution
741 in a mountain watershed. *Water Resources Research*, **36**(1), 13–26 (doi: 10.1029/1999WR900251)
- 742 Barry RG (1992) *Mountain weather and climate*. Cambridge University Press, 3rd edition
- 743 Beaumont RT and Work RA (1963) Snow sampling results from three samplers. *International Association of Scientific*
744 *Hydrology. Bulletin*, **8**(4), 74–78 (doi: 10.1080/02626666309493359)
- 745 Berthier E, Schiefer E, Clarke GK, Menounos B and Rémy F (2010) Contribution of Alaskan glaciers to sea-level
746 rise derived from satellite imagery. *Nature Geoscience*, **3**(2), 92–95
- 747 Burgess EW, Forster RR and Larsen CF (2013) Flow velocities of Alaskan glaciers. *Nature communications*, **4**,
748 2146–2154 (doi: 10.1038/ncomms3146)
- 749 Burnham KP and Anderson DR (2004) Multimodel Inference: Understanding AIC and BIC in Model Selection.
750 *Sociological Methods & Research*, **33**(2), 261–304 (doi: 10.1177/0049124104268644)
- 751 Carroll T (1977) A comparison of the CRREL 500 cm³ tube and the ILTS 200 and 100 cm³ box cutters used for
752 determining snow densities. *Journal of Glaciology*, **18**(79), 334–337 (doi: 10.1017/S0022143000021420)
- 753 Clark MP, Hendrikx J, Slater AG, Kavetski D, Anderson B, Cullen NJ, Kerr T, Örn Hreinsson E and Woods RA
754 (2011) Representing spatial variability of snow water equivalent in hydrologic and land-surface models: A review.
755 *Water Resources Research*, **47**(7) (doi: 10.1029/2011WR010745)
- 756 Clarke GK (2014) A short and somewhat personal history of Yukon glacier studies in the Twentieth Century. *Arctic*,
757 **37**(1), 1–21
- 758 Clyde GD (1932) Circular No. 99-Utah Snow Sampler and Scales for Measuring Water Content of Snow. *UAES*
759 *Circulars*, Paper 90
- 760 Cogley J, Hock R, Rasmussen L, Arendt A, Bauder A, Braithwaite R, Jansson P, Kaser G, Möller M, Nicholson L
761 and others (2011) *Glossary of glacier mass balance and related terms*. UNESCO-IHP, Paris
- 762 Conger SM and McClung DM (2009) Comparison of density cutters for snow profile observations. *Journal of*
763 *Glaciology*, **55**(189), 163–169 (doi: 10.3189/002214309788609038)
- 764 Crochet P, Jóhannesson T, Jónsson T, Sigurðrsson O, Björnsson H, Pálsson F and Barstad I (2007) Estimating
765 the Spatial Distribution of Precipitation in Iceland Using a Linear Model of Orographic Precipitation. *Journal of*
766 *Hydrometeorology*, **8**(6), 1285–1306 (doi: 10.1175/2007JHM795.1)

- 767 Crompton JW and Flowers GE (2016) Correlations of suspended sediment size with bedrock lithology and glacier
768 dynamics. *Annals of Glaciology*, **57**(72), 1–9 (doi: 10.1017/aog.2016.6)
- 769 Cullen NJ, Anderson B, Sirguey P, Stumm D, Mackintosh A, Conway JP, Horgan HJ, Dadić R, Fitzsimons SJ
770 and Lorrey A (2017) An 11-year record of mass balance of Brewster Glacier, New Zealand, determined using a
771 geostatistical approach. *Journal of Glaciology*, **63**(238), 199–217 (doi: 10.1017/jog.2016.128)
- 772 Dadić R, Mott R, Lehning M and Burlando P (2010) Parameterization for wind-induced preferential deposition of
773 snow. *Journal of Geophysical Research: Earth Surface*, **24**(14), 1994–2006 (doi: 10.1029/2009JF001261)
- 774 Danby RK, Hik DS, Slocombe DS and Williams A (2003) Science and the St. Elias: an evolving framework
775 for sustainability in North America’s highest mountains. *The Geographical Journal*, **169**(3), 191–204 (doi:
776 10.1111/1475-4959.00084)
- 777 Davis JC and Sampson RJ (1986) *Statistics and data analysis in geology*. Wiley New York et al., 2nd edition
- 778 Deems JS and Painter TH (2006) Lidar measurement of snow depth: accuracy and error sources. In *Proceedings of*
779 *the International Snow Science Workshop*
- 780 Dixon D and Boon S (2012) Comparison of the SnowHydro snow sampler with existing snow tube designs. *Hydrological*
781 *Processes*, **26**(17), 2555–2562 (doi: 10.1002/hyp.9317)
- 782 Egli L, Griessinger N and Jonas T (2011) Seasonal development of spatial snow-depth variability across different
783 scales in the Swiss Alps. *Annals of Glaciology*, **52**(58), 216–222 (doi: 10.3189/172756411797252211)
- 784 Elder K, Dozier J and Michaelsen J (1991) Snow accumulation and distribution in an alpine watershed. *Water*
785 *Resources Research*, **27**(7), 1541–1552 (doi: 10.1029/91WR00506)
- 786 Elder K, Rosenthal W and Davis RE (1998) Estimating the spatial distribution of snow water equiv-
787 alence in a montane watershed. *Hydrological Processes*, **12**(1011), 1793–1808 (doi: 10.1002/(SICI)1099-
788 1085(199808/09)12:10<111793::AID-HYP6953.0.CO;2-K)
- 789 Erxleben J, Elder K and Davis R (2002) Comparison of spatial interpolation methods for estimating snow distribution
790 in the Colorado Rocky Mountains. *Hydrological Processes*, **16**(18), 3627–3649 (doi: 10.1002/hyp.1239)
- 791 Fames PE, Peterson N, Goodison B and Richards RP (1982) Metrication of Manual Snow Sampling Equipment. In
792 *Proceedings of the 50th Western Snow Conference*, 120–132
- 793 Fierz C, Armstrong RL, Durand Y, Etchevers P, Greene E, McClung DM, Nishimura K, Satyawali PK and Sokratov
794 SA (2009) *The international classification for seasonal snow on the ground*. UNESCO/IHP, unesco/ihp paris
795 edition
- 796 Garbrecht J and Martz L (1994) Grid size dependency of parameters extracted from digital elevation models.
797 *Computers & Geosciences*, **20**(1), 85–87 (doi: 10.1016/0098-3004(94)90098-1)

- 798 Gerber F, Lehning M, Hoch SW and Mott R (2017) A close-ridge small-scale atmospheric flow field and its
799 influence on snow accumulation. *Journal of Geophysical Research: Atmospheres*, **122**(15), 7737–7754 (doi:
800 10.1002/2016JD026258), 2016JD026258
- 801 Grabiec M, Puczek D, Budzik T and Gajek G (2011) Snow distribution patterns on Svalbard glaciers derived from
802 radio-echo soundings. *Polish Polar Research*, **32**(4), 393–421 (doi: 10.2478/v10183-011-0026-4)
- 803 Gray DM and Male DH (1981) *Handbook of snow: principles, processes, management & use*. Pergamon Press, 1st
804 edition
- 805 Grünewald T, Schirmer M, Mott R and Lehning M (2010) Spatial and temporal variability of snow depth and ablation
806 rates in a small mountain catchment. *Cryosphere*, **4**(2), 215–225 (doi: 10.5194/tc-4-215-2010)
- 807 Grünewald T, Stötter J, Pomeroy J, Dadic R, Moreno Baños I, Marturià J, Spross M, Hopkinson C, Burlando P
808 and Lehning M (2013) Statistical modelling of the snow depth distribution in open alpine terrain. *Hydrology and*
809 *Earth System Sciences*, **17**(8), 3005–3021 (doi: 10.5194/hess-17-3005-2013)
- 810 Grünewald T, Bühler Y and Lehning M (2014) Elevation dependency of mountain snow depth. *The Cryosphere*, **8**(6),
811 2381–2394 (doi: 10.5194/tc-8-2381-2014)
- 812 Guo-an T, Yang-he H, Strobl J and Wang-qing L (2001) The impact of resolution on the accuracy of hydrologic data
813 derived from DEMs. *Journal of Geographical Sciences*, **11**(4), 393–401 (doi: 10.1007/BF02837966)
- 814 Gusmeroli A, Wolken GJ and Arendt AA (2014) Helicopter-borne radar imaging of snow cover on and around glaciers
815 in Alaska. *Annals of Glaciology*, **55**(67), 78–88 (doi: 10.3189/2014AoG67A029)
- 816 Hagen JO and Liestøl O (1990) Long-term glacier mass-balance investigations in Svalbard, 1950–88. *Annals of*
817 *Glaciology*, **14**(1), 102–106
- 818 Helbig N and van Herwijnen A (2017) Subgrid parameterization for snow depth over mountainous terrain from flat
819 field snow depth. *Water Resources Research*, **53**(2), 1444–1456 (doi: 10.1002/2016WR019872)
- 820 Hock R (2005) Glacier melt: a review of processes and their modelling. *Progress in Physical Geography*, **29**(3), 362–391
821 (doi: 10.1191/0309133305pp453ra)
- 822 Hock R and Jensen H (1999) Application of kriging interpolation for glacier mass balance computations. *Geografiska*
823 *Annaler: Series A, Physical Geography*, **81**(4), 611–619 (doi: 10.1111/1468-0459.00089)
- 824 Kaser G, Fountain A, Jansson P and others (2003) *A manual for monitoring the mass balance of mountain glaciers*.
825 ICSI/UNESCO
- 826 Kienzie S (2004) The Effect of DEM Raster Resolution on First Order, Second Order and Compound Terrain
827 Derivatives. *Transactions in GIS*, **8**(1), 83–111 (doi: 10.1111/j.1467-9671.2004.00169.x)
- 828 Kinar N and Pomeroy J (2015) Measurement of the physical properties of the snowpack. *Reviews of Geophysics*,
829 **53**(2), 481–544 (doi: 10.1002/2015RG000481)

- 830 Kohavi R and others (1995) A study of cross-validation and bootstrap for accuracy estimation and model selection.
831 In *Proceedings of the Fourteenth International Joint Conference on Artificial Intelligence*, 1137–1145
- 832 Korona J, Berthier E, Bernard M, Rémy F and Thouvenot E (2009) SPIRIT SPOT 5 stereoscopic survey of Polar
833 Ice: Reference images and topographies during the fourth International Polar Year (2007–2009). *ISPRS Journal*
834 *of Photogrammetry and Remote Sensing*, **64**(2), 204–212 (doi: 10.1016/j.isprsjprs.2008.10.005)
- 835 Lehning M, Völksch I, Gustafsson D, Nguyen TA, Stähli M and Zappa M (2006) ALPINE3D: a detailed model of
836 mountain surface processes and its application to snow hydrology. *Hydrological Processes*, **20**(10), 2111–2128 (doi:
837 10.1002/hyp.6204)
- 838 Li J and Heap AD (2008) A review of spatial interpolation methods for environmental scientists. *Geoscience Australia*,
839 Record 2008/23
- 840 Liston GE and Elder K (2006) A distributed snow-evolution modeling system (SnowModel). *Journal of*
841 *Hydrometeorology*, **7**(6), 1259–1276 (doi: 10.1175/JHM548.1)
- 842 Liston GE and Sturm M (1998) A snow-transport model for complex terrain. *Journal of Glaciology*, **44**(148), 498–516
- 843 López-Moreno J, Latron J and Lehmann A (2010) Effects of sample and grid size on the accuracy and stability of
844 regression-based snow interpolation methods. *Hydrological Processes*, **24**(14), 1914–1928 (doi: 10.1002/hyp.7564)
- 845 López-Moreno J, Fassnacht S, Heath J, Musselman K, Revuelto J, Latron J, Morán-Tejeda E and Jonas T (2013)
846 Small scale spatial variability of snow density and depth over complex alpine terrain: Implications for estimating
847 snow water equivalent. *Advances in Water Resources*, **55**, 40–52 (doi: 10.1016/j.advwatres.2012.08.010)
- 848 López-Moreno JJ, Fassnacht S, Beguería S and Latron J (2011) Variability of snow depth at the plot scale: implications
849 for mean depth estimation and sampling strategies. *The Cryosphere*, **5**(3), 617–629 (doi: 10.5194/tc-5-617-2011)
- 850 MacDougall AH and Flowers GE (2011) Spatial and temporal transferability of a distributed energy-balance glacier
851 melt model. *Journal of Climate*, **24**(5), 1480–1498 (doi: 10.1175/2010JCLI3821.1)
- 852 Machguth H, Eisen O, Paul F and Hoelzle M (2006) Strong spatial variability of snow accumulation observed
853 with helicopter-borne GPR on two adjacent alpine glaciers. *Geophysical Research Letters*, **33**(13), 1–5 (doi:
854 10.1029/2006GL026576)
- 855 Madigan D and Raftery AE (1994) Model Selection and Accounting for Model Uncertainty in Graphical Models
856 Using Occam’s Window. *Journal of the American Statistical Association*, **89**(428), 1535–1546
- 857 Marshall HP, Koh G, Sturm M, Johnson J, Demuth M, Landry C, Deems J and Gleason J (2006) Spatial variability of
858 the snowpack: Experiences with measurements at a wide range of length scales with several different high precision
859 instruments. In *Proceedings International Snow Science Workshop*, 359–364
- 860 McGrath D, Sass L, O’Neel S, Arendt A, Wolken G, Gusmeroli A, Kienholz C and McNeil C (2015) End-of-winter
861 snow depth variability on glaciers in Alaska. *Journal of Geophysical Research: Earth Surface*, **120**(8), 1530–1550
862 (doi: 10.1002/2015JF003539)

- Metropolis N and Ulam S (1949) The Monte Carlo Method. *Journal of the American Statistical Association*, **44**(247), 335–341
- Molotch N, Colee M, Bales R and Dozier J (2005) Estimating the spatial distribution of snow water equivalent in an alpine basin using binary regression tree models: the impact of digital elevation data and independent variable selection. *Hydrological Processes*, **19**(7), 1459–1479 (doi: 10.1002/hyp.5586)
- Mott R, Faure F, Lehning M, Löwe H, Hynek B, Michlmayer G, Prokop A and Schöner W (2008) Simulation of seasonal snow-cover distribution for glacierized sites on Sonnblick, Austria, with the Alpine3D model. *Annals of Glaciology*, **49**(1), 155–160 (doi: 10.3189/172756408787814924)
- Musselman KN, Pomeroy JW, Essery RL and Leroux N (2015) Impact of windflow calculations on simulations of alpine snow accumulation, redistribution and ablation. *Hydrological Processes*, **29**(18), 3983–3999 (doi: 10.1002/hyp.10595)
- Proksch M, Rutter N, Fierz C and Schneebeli M (2016) Intercomparison of snow density measurements: bias, precision, and vertical resolution. *The Cryosphere*, **10**(1), 371–384 (doi: 10.5194/tc-10-371-2016)
- Pulwinski A (2017) *Multi-scale investigation of winter balance on alpine glaciers*. Master’s thesis, Simon Fraser University
- Raftery AE, Madigan D and Hoeting JA (1997) Bayesian Model Averaging for Linear Regression Models. *Journal of the American Statistical Association*, **92**(437), 179–191 (doi: 10.1080/01621459.1997.10473615)
- Rasmussen CE and Williams CK (2006) *Gaussian processes for machine learning*. MIT press Cambridge
- Réveillet M, Vincent C, Six D and Rabatel A (2016) Which empirical model is best suited to simulate glacier mass balances? *Journal of Glaciology*, **63**(237), 1–16 (doi: 10.1017/jog.2016.110)
- Roustant O, Ginsbourger D and Deville Y (2012) DiceKriging, DiceOptim: Two R packages for the analysis of computer experiments by kriging-based metamodeling and optimization. *Journal of Statistical Software*, **21**, 1–55
- Schneiderbauer S and Prokop A (2011) The atmospheric snow-transport model: SnowDrift3D. *Journal of Glaciology*, **57**(203), 526–542 (doi: 10.3189/002214311796905677)
- Schuler TV, Crochet P, Hock R, Jackson M, Barstad I and Jóhannesson T (2008) Distribution of snow accumulation on the Svartisen ice cap, Norway, assessed by a model of orographic precipitation. *Hydrological Processes*, **22**(19), 3998–4008 (doi: 10.1002/hyp.7073)
- Scipión DE, Mott R, Lehning M, Schneebeli M and Berne A (2013) Seasonal small-scale spatial variability in alpine snowfall and snow accumulation. *Water Resources Research*, **49**(3), 1446–1457, ISSN 1944-7973 (doi: 10.1002/wrcr.20135)
- Shea C and Jamieson B (2010) Star: an efficient snow point-sampling method. *Annals of Glaciology*, **51**(54), 64–72 (doi: 10.3189/172756410791386463)

- 895 Sold L, Huss M, Hoelzle M, Anderegg H, Joerg PC and Zemp M (2013) Methodological approaches to
896 infer end-of-winter snow distribution on alpine glaciers. *Journal of Glaciology*, **59**(218), 1047–1059 (doi:
897 10.3189/2013JoG13J015)
- 898 Stein ML (1999) *Interpolation of spatial data: some theory for kriging*. Springer Science & Business Media
- 899 Tangborn WV, Krimmel RM and Meier MF (1975) A comparison of glacier mass balance by glaciological, hydrological
900 and mapping methods, South Cascade Glacier, Washington. *International Association of Hydrological Sciences*
901 *Publication*, **104**, 185–196
- 902 Taylor-Barge B (1969) *The summer climate of the St. Elias Mountain region*. Montreal: Arctic Institute of North
903 America, Research Paper No. 53
- 904 Thibert E, Blanc R, Vincent C and Eckert N (2008) Glaciological and volumetric mass-balance measurements: error
905 analysis over 51 years for Glacier de Sarennes, French Alps. *Journal of Glaciology*, **54**(186), 522–532
- 906 Trujillo E and Lehning M (2015) Theoretical analysis of errors when estimating snow distribution through point
907 measurements. *The Cryosphere*, **9**(3), 1249–1264 (doi: 10.5194/tc-9-1249-2015)
- 908 Turcan J and Loijens H (1975) Accuracy of snow survey data and errors in snow sampler measurements. In *32nd*
909 *Eastern Snow Conference*
- 910 Tveit J and Killingtveit Å (1994) Snow surveys for studies of water budget on Svalbard 1991–1994. In *Proceedings*
911 *of the 10th International Northern Research Basins Symposium and Workshop, Spitsbergen, Norway. SINTEF*
912 *Report*, volume 22, A96415
- 913 Waechter A, Copland L and Herdes E (2015) Modern glacier velocities across the Icefield Ranges, St Elias
914 Mountains, and variability at selected glaciers from 1959 to 2012. *Journal of Glaciology*, **61**(228), 624–634 (doi:
915 10.3189/2015JoG14J147)
- 916 Walmsley APU (2015) *Long-term observations of snow spatial distributions at Hellstugubreen and Gråsubreen,*
917 *Norway*. Master’s thesis, University of Oslo
- 918 Wetlaufer K, Hendrikx J and Marshall L (2016) Spatial Heterogeneity of Snow Density and Its Influence on Snow Wa-
919 ter Equivalence Estimates in a Large Mountainous Basin. *Hydrology*, **3**(3), 1–17 (doi: 10.3390/hydrology3010003)
- 920 Wilson N and Flowers G (2013) Environmental controls on the thermal structure of alpine glaciers. *The Cryosphere*,
921 **7**(1), 167–182 (doi: 10.5194/tc-7-167-2013)
- 922 Wilson NJ, Flowers GE and Mingo L (2013) Comparison of thermal structure and evolution between neighboring
923 subarctic glaciers. *Journal of Geophysical Research: Earth Surface*, **118**(3), 1443–1459 (doi: 10.1002/jgrf.20096)
- 924 Winstral A, Elder K and Davis RE (2002) Spatial snow modeling of wind-redistributed snow using terrain-based pa-
925 rameters. *Journal of Hydrometeorology*, **3**(5), 524–538 (doi: 10.1175/1525-7541(2002)0030524:SSMOWR2.0.CO;2)
- 926 Winstral A, Marks D and Gurney R (2013) Simulating wind-affected snow accumulations at catchment to basin
927 scales. *Advances in Water Resources*, **55**, 64–79 (doi: 10.1016/j.advwatres.2012.08.011)

- 928 Winther J, Bruland O, Sand K, Killingtveit A and Marechal D (1998) Snow accumulation distribution on Spitsbergen,
929 Svalbard, in 1997. *Polar Research*, **17**, 155–164 (doi: 10.3402/polar.v17i2.6616)
- 930 Woo MK and Marsh P (1978) Analysis of Error in the Determination of Snow Storage for Small High Arctic Basins.
931 *Journal of Applied Meteorology*, **17**(10), 1537–1541 (doi: 10.1175/1520-0450(1978)0171537:AOEITD2.0.CO;2)
- 932 Wood WA (1948) Project “Snow Cornice”: the establishment of the Seward Glacial research station. *Arctic*, **1**(2),
933 107–112
- 934 Work R, Stockwell H, Freeman T and Beaumont R (1965) *Accuracy of field snow surveys*. Cold Regions Research &
935 Engineering Laboratory
- 936 Zhang W and Montgomery DR (1994) Digital elevation model grid size, landscape representation, and hydrologic
937 simulations. *Water Resources Research*, **30**(4), 1019–1028 (doi: 10.1029/93WR03553)